Pontificia Universidad Católica de Chile
Doctorado en Neurociencias

Brain response to auditory deviance with and without conscious access

Doctoral thesis submitted to the Neuroscience program in partial compliance with the requirements to obtain the degree of Ph.D. in Neuroscience

by

Sergio Andrés Osorio Galeano

August 2022
Santiago de Chile

Advisor
Francisco Aboitiz, Ph.D.

Thesis committee
Vladimir López, Ph.D. (president)
Eugenio Rodríguez, Ph.D.
Pablo Billeke, Ph.D.

A mi familia
y al amor inquebrantable
que nos mantiene unidos
a pesar de la distancia

PONTIFICIA UNIVERSIDAD CATÓLICA DE CHILE
Facultad de Medicina - Facultad de Ciencias Biológicas
Facultad de Ciencias Sociales - Facultad de Química y de Farmacia
Doctorado en Neurociencias

El Comité de Tesis, constituido por los Profesores abajo firmantes, aprueba la Defensa Publica de la Tesis Doctoral titulada:

BRAIN RESPONSE TO AUDITORY DEVIANCE WITH AND WITHOUT CONSCIOUS ACCESS

Aprobación Defensa:

SERGIO OSORIO GALEANO

Calificándose el trabajo realizado, el manuscrito sometido y la defensa oral, con nota

7 (siete)

Dr. Mauricio Cuello
Director de Investigación y Doctorado
Escuela de Medicina
Pontificia Universidad Católica de Chile

Dr. Felipe Heusser
Decano
Facultad de Medicina
Pontificia Universidad Católica de Chile

Dra. Claudia Sáez
Sub-Directora
Dirección de Investigación y Doctorado
Escuela de Medicina
Pontificia Universidad Católica de Chile

Dr. Francisco Aboitiz D.
Director Tesis
Jefe Programa Doctorado en Neurociencias
Facultad de Medicina
Pontificia Universidad Católica de Chile

Dr. Eugenio Rodríguez
Evaluado Interno
Facultad de Medicina
Pontificia Universidad Católica de Chile

Dr. Vladimir López
Evaluado Interno
Facultad de Medicina
Pontificia Universidad Católica de Chile

Prof. Pablo Billeke
Profesor Evaluador
Universidad del Desarrollo

Santiago, 05 de agosto 2022

Acknowledgments

I dedicate this piece of work to Rosario, for her sweet vigilance and unconditional support. I held her hand as I walked into my first day of school, and I feel like I am holding it as I write these lines. To Ramón, whose biggest legacy will always be having taught his children the inestimable value of a good education. To my sister, Sandra, who has been a role model of discipline, perseverance, and excellence for as long as I have memory. And to my brother, Alex, who instilled in me the wit, curiosity, resolution, and the adventurousness without which I would never have dared to pursue a doctoral degree.

I would also like to thank Prof. Cristina Cadavid and Dr. Ana María Sierra, for showing me how academic rigor can go hand-in-hand with kindness and loving care. To Dr. Merel Keijzer, for inspiring me to become a researcher and for her crucial support in applying to this doctoral program. To Dr. Francisco Aboitiz, for welcoming me in his lab and providing the means and advice to become a junior scientist. To Dr. Lars Meyer, for advising me beyond academic matters and for showing me the meaning of scientific integrity. And to Dr. Yifei He and Dr. Florencia Assaneo, for kindly sharing their time, knowledge, and experience when this stranger knocked on their doors.

I also want to thank some friends and colleagues. Thanks to Luisa Cano, Sebastian Bedoya and Jonatan Castro, with whom I discovered my love for science. Thanks to Anders Thammawat, who offered emotional contention, intellectual support, and a cold beer during the sleepless summer nights spent preparing for final exams. To Martin Irani, who humbled me with his incredible talent for neuroscience and his

willingness to offer anyone a helping hand. To Vicente Medel, whose passion for science has always been an inspiration, and to Marcos Domic for being a fantastic colleague and unconditional friend. Thanks a lot to my course mates Carolina Gonzales, Ángeles Tepper, Catalina Fabar, Joaquín Valdés, and my lab mates Joaquín Herrero and Rosario Gajardo, with whom I shared struggles and whose friendship cheered me up in the hardest of moments. Special thanks to my soulmate, Ishani Thakkar, whose love, support, and company during these last years have been a soothing sunshine through good and difficult times.

Finally, I want to thank Dr. Rodrigo Henriquez, Dr. Tomás Ossandón and Dr. Gonzalo Boncompte, and the members of my thesis committee, Dr. Pablo Billeke, Dr. Eugenio Rodríguez, and Dr. Vladimir López for their scholarly contribution to the scientific quality of this piece of work. Many thanks to Agencia Nacional de Investigación y Desarrollo ANID, for funding my doctoral studies through the national grant n° 21181786, and to the School of Medicine and Pontificia Universidad Católica de Chile for hosting me during these years.

Content index

Figure index

Table index

List of abbreviations

ACC: Anterior Cingulate Cortex

dB: Decibels

d': D prime

dwPLI: Debiased weighted phase-lag index

EEG: Electroencephalography

ERP: Event-related potential

FC: Functional connectivity

FDR: False discovery rate

fMRI: Functional magnetic resonance imaging

GNW: Global Neuronal Workspace

Hz: Hertz

LC: Locus coeruleus

LORETA: Standardized low resolution brain electromagnetic tomography

MEG: Magnetoencephalography

MNI: Montreal Neurological Institute

MMN: Mismatch negativity

ms: Milliseconds

NE: Norepinephrine / Noradrenaline

pM/STG: Posterior middle and superior temporal gyrus

PCC: Posterior Cingulate Cortex

pINS/HG: posterior portion of the insular cortex and portions of the Heschl's gyrus

PFC: Prefrontal Cortex

SE: Standard error

SD: standard deviation

subDEV: subthreshold deviant

supraDEV: suprathreshold deviant

tgtSTD: target standard

1. Summary

The ability to extract statistical regularities in sensory stimuli and detect when those regularities are violated is of paramount importance for biological organisms, as they mediate autonomic and goal-directed responses that are crucial for survival. One the one hand, extraction of regularities in the sensory scene allows the consolidation of an internal model of the world. On the other, regularity violation allows the updating of such model, thus mediating behavioral adaptation.

In the field of auditory neuroscience, the brain response to sensory deviance in the auditory modality has been classically studied by mean of even-related potential (ERP) analyses. This literature has shown that the brain response to auditory deviance can be characterized by sequence of two neural responses: the mismatch negativity (MMN) and the P3 response. The MMN is an automatic neural event that can be observed regardless of conscious and attentional states, whereas the P3 crucially depends on conscious access to sensory deviance.

Two other potential markers of auditory deviance are phasic changes in pupil size (which reflects norepinephrine-mediated adaptation of arousal) and evoked power increases in the theta (4-7 Hz) and beta (15-30 Hz) frequency bands. While some literature shows that deviance detection is accompanied by increases in pupil size and theta and beta power, how these neural responses are modulated by conscious access to auditory deviance remains poorly understood. Understanding how the brain responds to auditory deviance with and without conscious access would be insightful as it would

shed some light on the dynamic interaction between bottom-up sensory processing and top-down modulatory mechanisms during goad-directed behavior.

In this study, we set out to understand how the brain responds to auditory deviance with and without conscious access. We designed a modified version of the auditory oddball task that allowed disentangling conscious from conscious processing of auditory deviance. We identified individual thresholds for conscious discrimination and then presented to our subjects sequences of tones where the last stimulus (i.e., the target) could be another standard tone, a subthreshold stimulus or a suprathreshold stimulus. Participants were required to report whether the target tone was the same or different from the preceding stimuli.

We collected behavioral (sensitivity indices and reaction times), pupillometric (evoked responses) and electroencephalography data (event-related potentials, time-frequency transformations at the scalp and source level, and functional connectivity) while participants performed our task. Results showed that subthreshold deviants were systematically and incorrectly judged as standard tones, thus reflecting subconscious processing of auditory deviance. In turn, suprathreshold targets were systematically and correctly judged as different, thus reflecting conscious access to deviance. We replicated well-established ERP findings showing that the sequence of MMN and P3 events can account for conscious and subconscious processing of auditory deviance. Pupillometric results show that while all target types elicit a phasic increase in pupil size, subconsciously processed deviant stimuli are associated with an increased pupil size within an early time window, thus reflecting unexpected sensory uncertainty. Theta and beta power were observed in cortical regions previously associated with the

MMN and the P3 events, including temporal, prefrontal, and cingulate cortices. While theta power increases in temporal regions reflect auditory predictions and stimulus-driven information maintenance, beta power increases in prefrontal and cingulate regions reflects sensory uncertainty and error detection. Finally, increased theta-band connectivity reflects information broadcasting about consciously accessed deviance to distributed neural processors, thus mediating accurate decision-making, whereas increased beta-band connectivity reflects top-down modulation due to uncertainty and saliency-driven error-detection mechanisms.

Our results highlight how the brain weighs bottom-up sensory processing and top-down mechanisms during goal-oriented behavior and the contribution of NE-mediated arousal adaptation to this process, which nicely illustrates the dynamic relationship between perception and cognition.

Resumen

La habilidad de extraer regularidades estadísticas presentes en estímulos sensoriales y detectar cuando se presentan violaciones a dichas regularidades es de vital importancia para los organismos biológicos, en tanto median respuestas autonómicas y dirigidas a metas que son cruciales para la supervivencia. Por un lado, la extracción de regularidades estadísticas presentes en la escena sensorial permite la consolidación de un modelo interno del mundo. Por otro, la detección de violaciones en estas regularidades permite la actualización de dicho modelo, mediando así procesos de adaptación conductual.

En el campo de la neurociencia cognitiva, la respuesta del cerebro a la desviación sensorial en la modalidad auditiva ha sido estudiada de manera clásica por medio de los potenciales asociados a eventos (ERPs, por su sigla en inglés). Esta literatura ha mostrado que la respuesta del cerebro a la desviación auditiva se puede caracterizar por la secuencia de dos respuestas neurales en la señal electroencefalográfica: el potencial de disparidad (MMN, por su sigla en inglés) y la respuesta P3. El MMN es un evento neural automático que puede ser observado independientemente de los estados atencionales o de consciencia de los individuos, mientras que la respuesta P3 depende crucialmente del acceso consciente a la desviación sensorial.

Otros dos potenciales marcadores de la desviación auditiva son los cambios fásicos en el tamaño de la pupila e incremento evocados en el poder oscilatorio de las bandas de frecuencia theta (4-7 Hz) y beta (15-30 Hz). Mientras la literatura muestra que la detección de la desviación está acompañada de incrementos en el tamaño de la

pupila (un marcador de la alerta y del sistema norepinefrinérgico) y del poder de theta y beta, no se conoce muy bien como estas respuestas neurales estarían moduladas por el acceso consciente a la desviación auditiva. Entender cómo responde el cerebro a la desviación auditiva con y sin acceso consciente nos permitiría entender la interacción dinámica existente entre mecanismos de procesamiento *bottom-up* y de modulación *top-down* durante el comportamiento enfocado a metas.

En este estudio, nos propusimos entender cómo responde el cerebro a la desviación auditiva con y sin acceso consciente. Para esto, diseñamos una versión modificada de la tarea clásica de tipo *oddball* auditivo que nos permitió separar el procesamiento consciente del procesamiento subconsciente de la desviación auditiva. Para esto, identificamos los umbrales de discriminación consciente de cada individuo, lo cual nos permitió presentar a nuestros sujetos secuencias de tonos donde el último estímulo (el estímulo objetivo), podía ser otro tono estándar, un estímulo subumbral o un estímulo supraumbral. Los participantes debían reportar si el último estímulo de cada secuencia había sido igual o distinto de los anteriores.

Por medio de esta tarea, recogimos datos conductuales (índices de sensibilidad y tiempos de reacción), pupilométricos (respuestas evocadas) y electroencefalográficos (ERPs, transformaciones de tiempo frecuencia al nivel de los electrodos y de las fuentes corticales, así como datos de conectividad funcional). Nuestros resultados muestran que las desviaciones subumbrales fueron incorrecta y sistemáticamente juzgadas como tonos estándar, lo cual refleja el procesamiento subconsciente de la desviación. En cambio, las desviaciones supraumbrales fueron correcta y sistemáticamente reportadas como diferentes, lo cual da cuenta del acceso consciente a la desviación auditiva.

Además, replicamos hallazgos sobre la secuencia de MMN y P3 como marcadores confiables del procesamiento consciente y subconsciente de la desviación. Los datos pupilométricos sugieren que todos los estímulos objetivos están asociados a una respuesta pupilar, pero que dicha respuesta es mayor durante el procesamiento subconsciente de la desviación auditiva, reflejando de esta manera el procesamiento de la incertidumbre perceptual inesperada. Incrementos en el poder de theta y beta fueron observados en regiones corticales previamente asociadas con los orígenes del MMN y P3, incluyendo regiones temporales, prefrontales y cinguladas. Mientras que el poder de theta en regiones temporales reflejaría predicciones auditivas y mantención de la información sobre la identidad de un estímulo auditivo novedoso, los incrementos en el poder de beta en regiones prefrontales y cinguladas reflejarían la detección de un error en la predicción y la incertidumbre sensorial. Finalmente, incrementos en la conectividad funcional dentro del rango de theta reflejarían intercambio de información entre procesadores corticales distribuidos globalmente, lo cual soportaría la percepción consciente y la toma de decisiones, mientras que incrementos de conectividad funcional dentro del rango de beta reflejarían procesos de modulación top-down señalando así la necesidad de adaptación de los niveles de alerta debido a una alta incertidumbre y mecanismos de detección de errores en la predicción que son sensibles a una mayor saliencia del evento sensorial.

Nuestros resultados subrayan como el cerebro asigna pesos a los mecanismos *bottom-up* y *top-down* durante el comportamiento enfocado a metas en función de si los eventos sensoriales son percibidos conscientemente o no, así como la contribución de la adaptación de la alerta durante esta interacción entre mecanismos de

procesamiento de la información sensorial. Eso ilustra además la relación dinámica y en constante adaptación entre percepción y cognición.

2. Introduction

2.1. Statistical regularities and regularity violations in sensory scene analysis

The ability to extract statistical regularities from sensory stimuli and to detect novel events that violate such inferred rules are ubiquitous characteristics of the brain that have direct implications for neural processing (Berkes et al., 2011; Ranganath & Rainer, 2003; Schapiro & Turk-Browne, 2015; Sohoglu & Chait, 2016; Tiitinen et al., 1994). Both of these capacities are systematically preserved across ontogeny and phylogeny, and can operate independently of intent or volition (Destrebecqz & Cleeremans, 2001; Schapiro & Turk-Browne, 2015). On the one hand, inference and learning of environmental statistical regularities facilitate the consolidation of an internal model of the world that can be compared against incoming information (Berkes et al., 2011; Friston, 2012; Kersten & Mamassian, 2004). In turn, detection of deviance from inferred statistical regularities allows the updating of such internal models, thus facilitating learning and behavioral adaptation (Friston, 2012; Friston & Kiebel, 2009; Ranganath & Rainer, 2003). Deviance detection is therefore a simple, yet extremely important mechanism for survival among biological organisms.

How the brain weighs the neural responses implicated in the detection of sensory deviance is in part determined by the physical properties of novel stimuli, which define its overall saliency, and global arousal levels and affect the readiness with which neural systems can process incoming information (Alamia et al., 2019; Näätänen et al., 2007; Polich, 1987, 2007; Teixeira et al., 2014). This highlights the fact that

bottom-up sensory mechanisms and top-down cognitive priors constantly and dynamically interact during goal-directed behavior (Aston-Jones & Cohen, 2005; Ferguson & Cardin, 2020; Nieuwenhuis et al., 2005). Because the mechanisms involved in deviance detection can operate independently of conscious perception but are at the same time involved in gating conscious access to behaviorally relevant information, understanding how the brain responds to sensory deviance with and without conscious access would provide insights into the dynamic relationship between perception and cognition.

2.2. Operationalizing conscious sensory experience

An overarching definition of consciousness is a huge and ongoing challenge for cognitive neuroscientists. Over the last decades, however, the Global Neuronal Workspace (GNW) hypothesis (Dehaene et al., 1998) has provided a useful framework and taxonomy to investigate the neural operations that underlie qualitatively different conscious states and experiences (Dehaene et al., 2006; Mashour et al., 2020). Under this framework, conscious experiences require the non-linear relay of information from local, modular processing units involved in early sensory processing to higher-order processors involved in a number of complex cognitive functions that are globally distributed across the brain (Baars, 1988; Dehaene et al., 1998, 2006; Mashour et al., 2020). This information relay is presumably implemented by the reciprocal long-range axon connections between local networks of sensory neurons in layers I and II and pyramidal neurons in layers II and III of the neocortex capable of gating, suppressing and broadcasting information inflow (Mashour et al., 2020). This hypothesis hence

grants a neurobiologically plausible framework to test and make predictions about the operations sustaining conscious experience.

An important distinction made in the context of the GNW hypothesis is that one between phenomenal and access consciousness. Phenomenal consciousness postulates the existence of conscious subjective experiences that are, however, not amenable to subjective report (Block, 2005; Naccache, 2018). Under this view, local activation of processing units in early sensory cortices without global information broadcasting is the defining principle that what should be considered conscious experience (Block, 2005). In contrast with this idea, access consciousness proposes that the accessibility of sensory information to prefrontal and parietal neuronal populations involved in cognitive control and allowing subjective report is the minimum requirement for conscious experience (Mashour et al., 2020; Naccache, 2018). Otherwise, GNW advocates claim, it would be problematic to disentangle conscious processing from other forms of sensory processing, such as subliminal, subconscious or preconscious processing, for which GNW offers an operational taxonomy (Dehaene et al., 2006).

In consonance with the GNW hypothesis, we here define conscious access as the availability of a reportable sensory experience (i.e., sensory deviance) for reasoning and rational decision making. Additionally, we label as subconscious processing (i.e., subliminal processing) any sensory experience that falls below perceptual thresholds, failing to trigger large-scale activation of distributed neural processors and, as a consequence, being non-amenable to conscious report (Dehaene et al., 2006; Mashour et al., 2020; Naccache, 2018). Another important distinction made under the GNW framework is that one between levels and contents of consciousness, with the former

standing for the mechanisms that sustain levels of brain activity necessary for information processing and the latter representing the mechanisms that facilitate the representation of percepts and their manipulation by cognition (Bachmann & Hudetz, 2014). In the context of this project, detection of sensory deviance is therefore an instantiation of a content of consciousness.

2.3. Event-related potentials and auditory deviance detection with and without conscious access

The processing of auditory deviance has been classically studied by means of Event-Related Potentials (ERPs) measured at the scalp level using Electroencephalography (EEG) during auditory oddball tasks (Bekinschtein et al., 2009; Kamp & Donchin, 2015; Linden, 2005; Näätänen et al., 2007; Polich, 2007). This line of research has demonstrated that the brain's response to auditory events that violate the statistics of preceding stimuli is characterized by the sequence of two neural events: The Mismatch Negativity (MMN) and the P3 response.

The MMN is a negative deflection in the ERP wave, peaking at around 200 milliseconds after the presentation of an odd stimulus (Näätänen et al., 2007, 2011; Tiitinen et al., 1994). This response has been shown to be independent of attentional state and conscious control (Bekinschtein et al., 2009; Näätänen et al., 2007, 2011; Tiitinen et al., 1994). Cortical generators have been identified in the middle and superior temporal gyri (M/STG) bilaterally, right prefrontal (PFC) regions, and anterior cingulate (ACC) regions (Garrido et al., 2009; Hyman et al., 2017; Rinne et al., 2000). Moreover, pharmacological studies have consistently shown that the MMN response

is sensitive to Glutamatergic modulations, as the use of ketamine, an antagonist of NMDA receptors, drastically reduces the amplitude of this ERP component (Ehrlichman et al., 2008; Heekeren et al., 2008; Javitt et al., 1996). The MMN has been suggested to reflect automatic generation of sensory memory traces and detection of mismatching representations in early auditory cortices (Fischer et al., 1999; Garrido et al., 2009; Näätänen et al., 2007, 2011).

When deviance is consciously accessed, a sustained positive deflection in the mean ERP response is observed, starting at around 300 (Polich, 1987, 2007; Sutton et al., 1965). In contrast to the MMN, the P3 is sensitive to attentional state and conscious detection, and its amplitude can be modulated by the physical properties of the novel stimulus (Comerchero & Polich, 1999; El Karoui et al., 2015; Polich, 2007; Ranganath & Rainer, 2003; Sutton et al., 1965). The P3 effect has further been dissected into two separate subcomponents that reflect different stages of information processing: an early P3a, which can be observed in frontocentral electrodes at the scalp level and is believed to originate in the prefrontal cortex, and a P3b, which can be observed in centroparietal electrodes and is believed to originate in a distributed network of cingulo-centro-parietal regions (El Karoui et al., 2015; Li et al., 2009; Linden, 2005; Polich, 2007). This has led to the proposal that the P3a reflects attention-dependent, stimulus-evaluation processes, while the P3b reflects context updating and information maintenance during deployment of working memory (Comerchero & Polich, 1999; Masson et al., 2018; Polich, 2007; Ranganath & Rainer, 2003). Additionally, multiple experiments in animal models have shown that the P3 response is highly sensitive to changes in the neuromodulator norepinephrine (Aston-Jones & Cohen, 2005; Murphy

et al., 2011; Nieuwenhuis et al., 2005). Pharmacological studies using clonidine, an α_2-adrenergic receptor agonist, and non-human primate lesion studies targeting the Locus Coeruleus (LC), a subcortical nucleus critical for noradrenergic modulation, have shown how neuromodulator norepinephrine causally contributes to the amplitude of the P3 responses (Pineda et al., 1989; Swick et al., 1994). However, other line of studies also suggests that dopaminergic deficits among Parkinson disease patients and administration of dopamine antagonist agents are also associated with a hampered P3 response (Polich & Criado, 2006; Takeshita & Ogura, 1994).

The vast literature and multiple replication studies on the sequence of these ERP responses in the auditory modality confirm that the MMN and the P3, including the P3a and P3b subcomponents, are reliable markers of conscious and subconscious processing of auditory deviance.

2.4. The pupil dilation response during detection of novel auditory events

Changes in pupil size are thought to partially reflect tonic and phasic release of the neuromodulator Norepinephrine (NE). Activity of noradrenergic neurons in the Locus Coeruleus (LC), targeting widespread regions in the frontal and parietal cortices, has been shown the precede tonal and phasic fluctuation in pupil size, both during rest as well as during task engagement (Aston-Jones & Cohen, 2005; Jodo et al., 1998; Vazey et al., 2018). NE presumably modulates cortical excitation-inhibition balances that regulate global arousal levels, hence gating perception and action (Aston-Jones & Cohen, 2005; Joshi et al., 2016; Nieuwenhuis et al., 2005; Vazey et al., 2018). Because the pupil is proxy of NE modulation of cortical states via arousal adaptation,

understanding how phasic increases in pupil size are modulated by conscious access to deviance could help us understand the relationship between brains states and conscious sensory experiences.

Previous studies have shown that the pupil is sensitive to the processing of auditory deviance. A phasic increase in pupil size has been associated with subjects' conscious processing of single auditory stimuli, but not to auditory stimuli that are not consciously perceived and reported (Bala et al., 2020). Similarly, consciously detected and correctly reported regularity violations within auditory sequences elicit a pupil response during active-counting and passive listening conditions, whereas violations that escape conscious perception do not elicit such response (Quirins et al., 2018). This has led to the proposal that the pupil response is a marker of conscious access to auditory novelty.

In sharp contrast, others have found that whether a pupil response is elicited crucially depends on the behavioral relevance of a target stimulus. Using a three-oddball paradigm, Liao and colleagues showed that only the most salient of two deviant stimuli elicits a pupil response during passive listening, even when both oddballs are above participants' perceptual thresholds. However, once subjects are required to monitor any change in the sensory scene, all deviant stimuli elicit a pupil response (Liao et al., 2016). Similarly, using complex sequences of tonal stimuli where auditory deviance was structural, Zhao and colleagues demonstrated that upon passive listening, only abrupt regularity violations of sequence structure elicit a pupil response. However, after asking participants to report any change in the auditory scene, both regularity violation and the emergence of new structural patterns in auditory sequences produce

a phasic increase in pupil size (Zhao et al., 2019). This line of evidence therefore suggests that rather than conscious access, the pupil response reflects adaptation of internal brain states that are sensitive to behaviorally relevant changes in the sensory scene. Therefore, whether pupil responses indeed reflect conscious access to sensory deviance is contentious. Unfortunately, none of the studies above explicitly addressed this research question.

2.5. Brain oscillations as markers of conscious perception and error detection

Brain oscillations with stereotypical frequency components are ubiquitous features of brain functioning that are remarkably well-preserved across multiple species regardless of brain size variability (Buzsáki et al., 2013). This hierarchical system of brain oscillation is thought to underlie brain organization, information maintenance, and local-global integration between distributed neuronal populations that fire either together or in antiphase within functionally relevant time windows (Buzsaki, 2006; Buzsáki, 2010). Thus, ongoing research up to the day links oscillatory activity within the delta (0.5-4 Hz), theta (4-8Hz), alpha (9-12), beta (13-30 Hz), low gamma (30-70 Hz) and high gamma (>70 Hz) bands have been previously associated with a variety of brain states and cognitive functions (Bastos et al., 2021; Buzsaki, 2006; Buzsáki, 2010; Engel et al., 2001; Engel & Singer, 2001; Fries, 2015; Miller et al., 2018; Sadaghiani & Kleinschmidt, 2016)

Two other potential markers of auditory deviance detection are evoked changes in oscillatory power within the range of theta (4-8Hz) and beta (15-30 Hz) oscillations.

Previous Magnetoencephalography (MEG) research has shown that auditory deviance detection is associated with increased theta power in bilateral source-reconstructed Middle and Superior Temporal Gyrus (M/STG), the prefrontal cortex (PFC) and hippocampal regions (Recasens et al., 2018). Using the same data-acquisition technique, Hsiao and colleagues reported increases in theta power and phase-locking in bilateral M/STG regions in response to auditory deviance (Hsiao et al., 2009). This is consistent with EEG studies which demonstrate that the MMN and the P3a responses are characterized by increased Theta power at the scalp level among healthy subjects, and with decreased theta power among Schizophrenic patients (Javitt et al., 2018; Solís-Vivanco et al., 2021). Theta-band activity, as well as nested theta-gamma cross-frequency interactions, have been previously associated with attentional sampling, memory-related computations, and conscious access to sensory events (Fries, 2015; Klimesch et al., 2001; Slagter et al., 2009).

Studies using intracranial recordings have also documented an increase in beta (13-25Hz) band power in temporal regions and decreased of activity within the same frequency band in prefrontal regions among epileptic patients upon auditory deviant detection (El Karoui et al., 2015). Stimuli that violate temporal predictions also elicit a coupling of delta (1-3Hz) and beta oscillations that biases perception and behavioral responses towards correct answers (Arnal et al., 2015). In line with this, others have observed an increase in low beta (15-20) power between 200 and 300 ms after the presentation of unpredicted pitch changes in sequences of tones (Chang et al., 2016). Such studies highlight a potential role of beta oscillations in encoding sensory predictions and stimulus uncertainty. Moreover, beta-band activity, and beta-alpha

cross-frequency dynamics, have been also linked to top-down control and attentional gating via feedback projections from prefrontal and parietal regions to primary sensory cortices (Bastos et al., 2018; Miller et al., 2018). Similar to pupil responses, how conscious access to auditory deviance modulates these evoked oscillatory events remains relatively understudied.

2.6. Summary and motivation for the present study

Detection of regularity violations in sensory scene analysis is an important mechanism that mediates adaptive and goal-directed behavior. Both stimulus properties and brain states can impact the neural responses to sensory deviance, but less is understood about how the brain responds to auditory deviance with and without conscious access. Understanding this is relevant because it would allow us to gain insights into the dynamic relationship between bottom-up sensory processing and top-down modulation. Previous research has demonstrated that the sequences of auditory ERP potentials are reliable markers of conscious and subconscious processing of auditory deviance. Pupil size and oscillatory dynamics stand as two potential markers of auditory deviance detection, but how they are modulated by conscious access is not well understood.

In this project, we investigate the brain response to auditory deviance with and without conscious access. Twenty-eight healthy subjects performed a modified version of the auditory oddball task designed to disentangle conscious from subconscious processing of auditory deviance. We collected behavioral, scalp electrophysiological and pupillometric data to investigate how these markers are differentially modulated

by conscious access. We computed reaction times, accuracy rates, ERP and evoked pupil responses. Moreover, we implemented source imaging analyses to inspect the spatial cortical activation dynamics associated to both types of processing. We also conducted time-frequency analyses at the scalp level and in source space to characterize the oscillatory dynamics underlying the processing of auditory deviance with and without conscious access. Finally, we estimated Functional Connectivity (FC) in the theta (4-8 Hz) and beta (15-30 Hz) frequency bands between temporal, frontal, and cingulate regions to understand how the brain weighs bottom-up and top-down signals during the processing of auditory deviance. Our experimental and analytic protocol is summarized in figure 1.

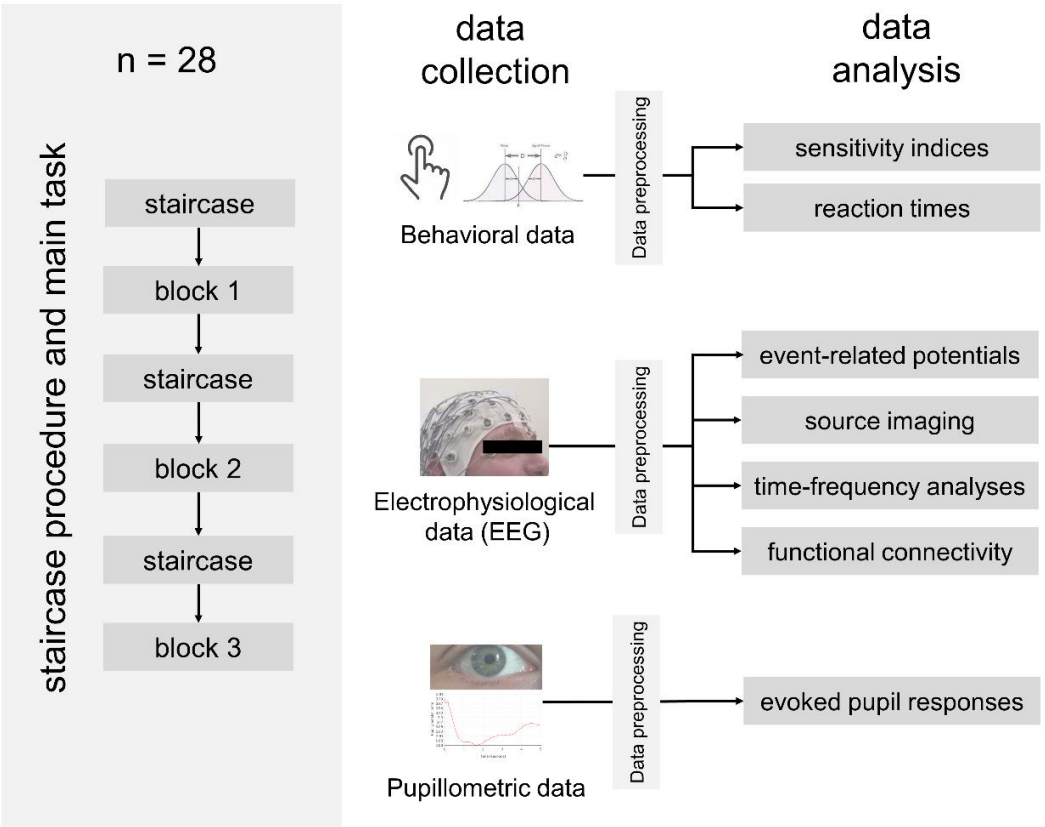

Figure 1. Schematic representation of our experimental and analytical protocol. Twenty-eight participants performed three blocks of our task, each preceded by a staircase procedure. Behavioral, electrophysiological and pupillometric data was collected, preprocessed, and analyzed.

3. Objectives

3.1. General Objective

To characterize the brain dynamics associated to the processing auditory deviance with and without conscious access.

3.2. Specific objectives

1) Design and test a behavioral paradigm that objectively disentangles conscious from subconscious processing of auditory deviance.
2) Replicate previous ERP findings on the processing of auditory deviance with and without conscious access.
3) Establish the spatial cortical activation dynamics associated to the processing of auditory deviance with and without conscious access.
4) Identify the pupillary dynamics associated to the processing of auditory deviance with and without conscious access.
5) Identify the oscillatory dynamics that underlie the processing of auditory deviance with and without conscious access.
6) Identify the functional connectivity patterns that characterize the processing of auditory deviance with and without conscious access.

4. Hypothesis

4.1. General Hypothesis

Conscious and subconscious processing of auditory deviance will feature neural dynamics which reflect two possible states in the interplay between bottom-up sensory processing and top-down modulatory mechanisms. While conscious access of auditory deviance will predominantly reflect bottom-up signals resulting from unambiguous sensory experience, subconscious processing auditory deviance will be characterized by increased top-down modulation resulting from higher perceptual uncertainty.

4.2. Working hypotheses

1) Conscious and subconscious processing of auditory deviance will elicit an MMN response, whereas only consciously perceived deviance will elicit a P3 response.
2) Both conscious and subconscious processing of auditory deviance will be associated to an increase in the pupil response, albeit of different amplitude, with consciously perceived deviants eliciting a more pronounced response than subconsciously perceived ones.
3) Conscious processing of auditory deviance will be associated with an increase in theta (4-8Hz) power in temporal regions whereas subconscious processing of auditory novelty will be associated with an increase in beta (15-30 Hz) power in prefrontal regions.

4) Conscious processing of auditory deviance will be characterized by increased functional connectivity between prefrontal, temporal, and cingulate regions within the theta (4-8 Hz) frequency band, whereas subconscious processing will feature increased functional connectivity within the beta (15-30 Hz) frequency band.

5. Methods

5.1. Participants

Twenty-eight right-handed subjects (16 females) with no self-reported record of auditory, neurological, or neuropsychiatric disorders voluntarily agreed to participate in this study (mean age = 25.92, SD = 3.10). All participants reported normal hearing and normal or corrected-to-normal vision. Subjects with extensive and/or formal musical training (> year) were not considered for the study. Participants were recruited from among the undergraduate and postgraduate community at Pontificia Universidad Católica de Chile and Universidad de Chile. Protocol and procedures were reviewed, approved, and supervised by the ethics committee for life and medical sciences at Pontificia Universidad Católica de Chile.

5.2. Procedures and stimuli

Participants sat 50 centimeters away from of a screen within a Faraday cage in a silent, dimly-lit room. Brain activity was recorded using a 64-channel Biosemi EEG system and pupil size was recorded using an Eyelink 1000 eye-tracker that was calibrated at the beginning of the experimental session. 150-millisecond long narrowband sinusoidal tones were presented binaurally via special airtube earphones (ER-1 Etymotic Research) with an interstimulus interval of 150 ms. All stimuli were created using Audacity and set to be delivered at an intensity of 70dBs. The task was programmed and presented using Presentation (NeuroBehavioral Systems, NBS).

The experiment included a 15-minute training session and three experimental blocks of ~15 minutes each. At the beginning of each experimental block, participants performed a staircase procedure (annex 1). This procedure allowed identifying subject-specific conscious discrimination thresholds and setting subthreshold tonal stimuli for the main task adaptively and according to individual hearing abilities. For the staircase procedure, a set of sixteen tonal stimuli were used per block with a base frequency of 800Hz, 1000Hz or 1200Hz (annex 2). Then, participants performed one of the three blocks in the main task. Each block in the main task included 270 trials, for 90 targets (30 per condition). Nine participants performed a longer version of the task (320 trials, 120 targets, 40 per condition).

In the main task (figure 2), participants were instructed to listen carefully to a series of standard tones and decide whether the last stimulus in each sequence was the same or different from the preceding stimuli. The number of standard tones before each target stimulus randomly varied between three and five tones. Participants reported their decision by pressing one of two buttons upon appearance of a prompt on screen 1,000 milliseconds after target onset. There was no time limit for response and participants were told to prioritize response accuracy over response speed. For each block, standard tones were presented at one of the base frequencies used for the staircase procedure. Target stimuli could be either another standard tone (tgtSTD), a tone that was 50 Hz above the base frequency (supraDEV) or a tone that was below each participants' discriminatory threshold (subDEV), as established during the staircase procedure before the beginning of the block for each subject. The theoretical probability for each type of target was 33.333%.

5.3. Behavioral data analysis

Behavioral data was obtained using Presentation (NeuroBehavioral Systems, NBS). Default logfiles were preprocessed and analyzed using in-house MATLAB scripts. We resorted to Signal Detection Theory (Green & Swets, 1966) to estimate sensitivity indices (*d'*). Sensitivity is a measure of target detectability (signal) that considers both error rates (noise) and response systematicity (bias), thus outperforming raw accuracy and hit probabilities in accounting for human decision-making processes in perceptual tasks (Kingdom & Prins, 2016). Sensitivity (*d'*) values were calculated for each target type by measuring the distance between mean number of correct responses and incorrect responses in standard deviation units, while correcting for perfect rates according to the 1/2N rule (Green & Swets, 1966; Hautus et al., 2022). Sensitivity values were obtained per block and then averaged across blocks per participant. Positive *d'* values suggest a higher proportion of correct over incorrect responses, whereas negative values suggest the opposite pattern. The farther away from zero, the lesser the probability that performance is due to chance. Data from one participant was rejected from all further analyses due to an erratic performance during the staircase procedure which resulted in unreliable discriminatory thresholds. Except for sensitivity, all subsequent analyses were carried out for tgtSTD and supraDEV trials followed by correct responses, and for subDEV trials followed by incorrect responses (percent rejected: tgtSTD, mean = 2.04 %, SD = 10.24 %; subDEV, mean = 16.76 %, SD = 29.31 %). Reaction times were calculated by subtracting the 1,000 ms time-window between target onset and response prompt from the participant's actual

response time. Any negative reaction time was considered a false alarm and was therefore rejected, along with outliers below and above the 2.5 and 97.5 percentiles in the data (percent rejected: tgtSTD-correct, mean = 3.70 %, SD = 0.96 %; subDEV-incorrect, mean = 3.02 %, SD = 1.22 %; supraDEV-correct, mean = 3.82 %, SD = 0.77 %). Because reaction time data was non-normally distributed, we computed median instead of mean reaction time values.

5.4. EEG data preprocessing and analysis

Electroencephalographic data was acquired at a sampling rate of 1,024 Hz. After acquisition, the signal was preprocessed using Brainstorm (Tadel et al., 2011). The continuous EEG signal was linearly detrended and noisy segments were rejected. Next, the EEG signal was re-referenced to the average of all electrodes and band-passed filtered between 1 and 45Hz using an FIR Keiser filter (Filter order = 37124, Stopband attenuation = 60dB) as implemented in the Brainstorm toolbox. Artifacts were removed using Independent Component Analysis (ICA, Makeig et al., 1996) on the continuous EEG signal prior to data segmentation (mean number of rejected components = 8.77, *SD* = 2.69). ICA was conducted using the Infomax algorithm by sorting the signal in 20 components. Artefactual components due to blinks and ocular movements were visually identified based on their topographical features and covariance with oculomotor and blink events observed in EOG time-series data. Components reflecting EMG or single-channel external noise were identified by visual inspection. Data was subsequently epoqued between -2,500ms and after 2,500ms upon target stimulus presentation. A trial-by-trial visual inspection was carried out to identify and reject bad

channels (mean = 1.00, SD = 1.15). Next, an automatic trail rejection procedure was performed, marking as bad any trial where EEG signal exceeded 100 microvolts in amplitude (mean = 7.25, SD = 7.15 including manual and automatic rejection).

Epoqued data was imported into MATLAB and store in data structures containing information about target type, response type, and sensitivity values. EEG data was downsampled to 250 Hz and mean Event Related Potentials were computed as the baseline-corrected average across subjects for tgtSTD-correct, subDEV-incorrect, and supraDEV-correct trials. Baseline correction was applied by subtracting the mean ERP between -500 milliseconds and time zero. Time-frequency wavelet decomposition analyses were conducted using the fieldtrip toolbox (Oostenveld et al., 2011), by means of a 7-cycle wavelet in steps of 0.5 Hz between 1 and 30 Hz, for a time window of -1500 to 1500 in steps of 20 ms. The grand average for tgtSTD-correct, subDEV-incorrect, supraDEV-correct trials was obtained and dB-normalized using a baseline period of -500 to -100 ms. EEG data from one participant was incomplete due to technical problems during acquisition and had to be rejected from analyses.

EEG forward models were computed using the symmetric Boundary Method BEM by the open-source software OpenMEEG (Gramfort et al., 2010) and signals were projected on the default MNI/ICMB152 cortical templates (Fonov et al., 2009) provided by the Brainstorm toolbox using a total number of 15,002 vertices. Source estimation was performed using the Standardized Low-Resolution Electromagnetic Tomography (sLORETA) method (Pasqual-Marqui, 2002), according to the Minimum Norm solution and using unconstrained sources. Empirical noise covariance was estimated from the recordings using approximately 1,000 ms baseline periods on each

trial, between approximately -2,500 and -1,500 ms prior to target onset. These empirical noise covariance matrices were used for noise covariance regularization. Since unconstrained sources return dipole triplets with orthogonal orientation, dipole reduction was conducted by estimating the norm of the vectorial sum of the three dipole orientations at each vertex (Tadel et al., 2011).

To obtain wavelet time-frequency transformations of source reconstructed signals, we repeated the same source-modelling procedure as above but this time using MNE Python toolbox (Gramfort et al., 2013). We then used Seven Network atlas (Schaefer et al., 2018) to subdivide the cortical surface into 100 parcellations and estimated the average signal for each parcellation as the mean of the norm of the three dipole orientations at each vertex within such parcellation. Data from each cortical source was then exported back to MATLAB and time-frequency analyses were implemented using the Fieldtrip toolbox. For each one of the 100 cortical parcels, data was downsampled to 250 Hz and wavelet analyses were conducted using a 7-cycle wavelet in steps of 0.33 Hz between 1 and 31 Hz, for a time window of -2,500 to 2,500 ms, in steps of 20 ms. dB normalization was performed as above, using the same baseline period of -500 to -100 ms.

For functional connectivity analyses, source-reconstructed data was imported into MATLAB, baseline corrected between -500 and 0 ms, and downsampled to 250 Hz. Time-frequency transformation was implemented in Fieldtrip using the Multitaper Frequency Transformation Method (mtmfft). Frequencies of interest were set from 1 to 31 Hz for two separate time windows: 0-250 ms and 250-500 ms, with a spectral smoothing of 8 Hz. Next, functional connectivity was estimated using the debiased

Weighted Phase-Lag Index (Vinck et al., 2011) as implemented in the Fieldtrip Toolbox and stored in adjacency The 100 parcels obtained from the Schaefer's seven network atlas were regrouped and relabeled according to their anatomical localization.

5.5. Pupillometry

Pupil data was acquired using Eyelinks' acquisition software at a sampling rate of 1000 Hz. Calibration procedures were carried out at the beginning of each experimental session. Pupil area, horizontal and vertical gaze positions were recorded from the right eye of each participant. Blinks and gaze artifacts were detected by Eyelinks' default algorithms. Pupil data was preprocessed using Anne Urai's pupil toolbox (Urai et al., 2017) plus additional custom MATLAB scrips. Eyelink-defined and additionally detected blinks were padded by 150 milliseconds and linearly interpolated. The pupil response evoked by blinks and saccadic events was identified via deconvolution and removed using linear regression (Knapen et al., 2016). The signal was then filtered between 0.01 Hz and 10 Hz using a second-order Butterworth filter and then down sampled to 250 Hz. Data was epoqued between 2500 milliseconds before and 2500 milliseconds after the onset of target stimuli and trials where pupil size was below and above the 0.5 and the 99.5 percentiles of each participants data were rejected. Data was subsequently z-normalized and the grand average of the pupil size for tgtSTD-correct, subDEV-incorrect, and supraDEV-correct trials was estimated. The time window for baseline correction comprised -500 milliseconds to time zero. Pupil data from three participants was unavailable due to problems during data acquisition.

5.6. Statistics

Non-parametric permutation statistics for behavioral data were implemented using custom-made MATLAB scripts. For *d'* and reaction times, we used a one-sample t-tests and non-parametric permutation procedures. For permutation procedures, the median values across conditions were obtained from the observed data. Next, we created a null distribution by exchanging condition levels over each iteration of a 10,000-permutation procedure. Then, observed values were compared against the percentiles corresponding to the Bonferroni-corrected alpha values obtained from the null distribution, and corresponding p-values were calculated. Bootstrapping procedures were similarly implemented, except that instead of interchanging labels across conditions, n values were randomly sampled (with replacement) from the observed values per condition for each iteration.

For time series data such as EEG and Pupil ERPs, we implemented the same procedure over time; that is, sample-by-sample with an additional criterion that for an effect to be significant, below-threshold p values should be observed for at least five continuous samples. For event-related potentials, we performed this analysis within *a priori* selected time windows, corresponding to the approximate latency of the MMN (150-250 ms) and the P3 (280-380 ms). Given our strongly directional hypotheses, we used one-tailed Bonferroni-corrected alpha values. For pupil data, however, we did not have a strong directionally hypothesis or predefined time windows of interest informed by the literature, and therefore performed two-tailed analyses between a bigger time window comprising 0 and 1,500 ms.

For scalp time-frequency data, two-tailed cluster-corrected statistics were obtained via a non-parametric, dependent samples permutation procedure (10,000 permutations) using the Fieldtrip toolbox (Oostenveld et al., 2011) between 150-250 ms and 280-380 ms. For all cluster-statistics, clustering of neighboring channels was set using the triangulation method and the uncorrected p-value for cluster inclusion was set at $p < 0.05$. Cluster significance probability was corrected using the Monte-Carlo method ($\alpha = 0.05$), for 10,000 permutations and a minimum number of neighboring channels of three.

For source-reconstructed time-frequency data, one-tailed cluster corrected statistics were obtained by means of a non-parametric permutation procedure (10,000 permutations, $\alpha = 0.05$) using custom-made MATLAB scripts. We compared the mean time-frequency response for subDEV-incorrect and supraDEV-correct trials and subtracted from them the mean response to tgtSTD-correct trials. The multiple comparison problem was addressed by using cluster correction, according to maximum cluster size value observed per permutation. Because there is bias in lower frequency towards bigger cluster size, we carried out this statistical procedure in two separate frequency intervals, first between 3 and 20 Hz, and then between 15 and 30 Hz. This resulted in a set of six regions showing a statistically significant effect. Because these regions were specified in terms of the network they belonged to, we relabeled then according to their anatomical localization. Annex 3 shows the localization of the regions that survived the permutation procedure in the MNI ICBM/152 cortical template.

For functional connectivity, we analyzed the mean difference between subDEV-incorrect and supraDEV-correct against tgtSTD-correct trials. We implemented a permutation procedure, shuffling condition labels over 5,000 iterations per parcellation. We thus obtained a null distribution of debiased wPLI values per region of interest, estimated the 2.5 and 97.5 percentiles in the null data corresponding to an $\alpha = 0.05$ for two-tailed analyses, and finally filtered out from the observed data any wPLI values that were less extreme that the critical values obtained from the null distributions (annex 4). We performed this procedure for both frequency intervals of interest (theta, 4-8 Hz and beta, 15-30 Hz). We regrouped the different parcellations from the 7-Network atlas according to their anatomical localization (cingulate, insular, occipital, prefrontal, parietal, temporal and somatomotor). Then, we obtained the mean dwPLI difference from tgtSTD-correct trials per region. Finally, we compared mean dwPLI for fronto-temporal, cingulo-temporal, and fronto-cingular functional connectivity for subDEV-incorrect and supraDEV-correct trials per cerebral hemisphere separately, using dependent sample t-tests. The multiple-comparison problem was addressed using FDR correction.

All Spearman correlation analyses were implemented using MATLAB's statistics toolbox default function (two-tailed testing).

6. Results

6.1. Behavioral results

We estimated sensitivity indices, also known as d prime (*d'*) values, for tgtSTD, subDEV and supraDEV targets across blocks and participants. We expected systematic and correct identification of non-novel standards (tgtSTD) and suprathreshold deviant targets (supraDEV), which should be reflected by positive *d'* values. In contrast, we expected participants to systematically and incorrectly judge subthreshold deviant targets (subDEV) as standard tones, which should be reflected by negative *d'* values. Figure 2b shows individual and group median sensitivity values for the three types of target stimuli. In line with our expectations, tgtSTD (*d'* = 3.30, SD = 0.99) and supraDEV targets were associated with positive *d'* values (*d'* = 4.26, SD = 0.66), whereas subDEV targets were associated with negative values (*d'* = -2.27, SD = 0.96). A one sample t-test (n = 27, two-tailed) showed that median sensitivity values statistically differed from zero (tgtSTD, $t = 16.48$, $p < 0.001$; subDEV, $t = 31.05$, $p < 0.001$; supraDEV, $t = -11.31$, $p < 0.001$). This suggests that, on average, supraDEV targets were consciously accessed as deviant stimuli, but that subDEV targets were subconsciously processed, but not consciously accessed as deviant. A non-parametric permutation procedure showed that the median *d'* statistically differed across conditions (figure 2b, n = 27, 10,000 permutations, two-tailed, Bonferroni-corrected, $p < 0.001$).

We next investigated reaction times (RT) to trials conforming to these target-response combinations. Figure 2c shows the median RT for tgtSTD-correct (median =

828.30, SD = 222.65), subDEV-incorrect (877.30, SD = 189.58) and supraDEV-correct trials (median = 742.90, SD =238.57). We then subtracted the median RT to tgtSTD-correct trials from the other two conditions (figure 2d). This allowed us to understand whether decision-making processes to subDEV-incorrect and supraDEV-correct trials were slower or faster compared to our baseline condition. Results showed that RTs to subDEV-incorrect trials were marginally slower (4.5 ms) than the median RTs to tgtSTD-correct, whereas supraDEV-correct targets were, on average, 37.45 ms faster than the median RT to tgtSTD-correct trials. A permutation test showed that the median RT difference effect was statistically significant at the group level (n = 27, 10,000 permutations, two-tailed, p = 0.0016, figure 2d).

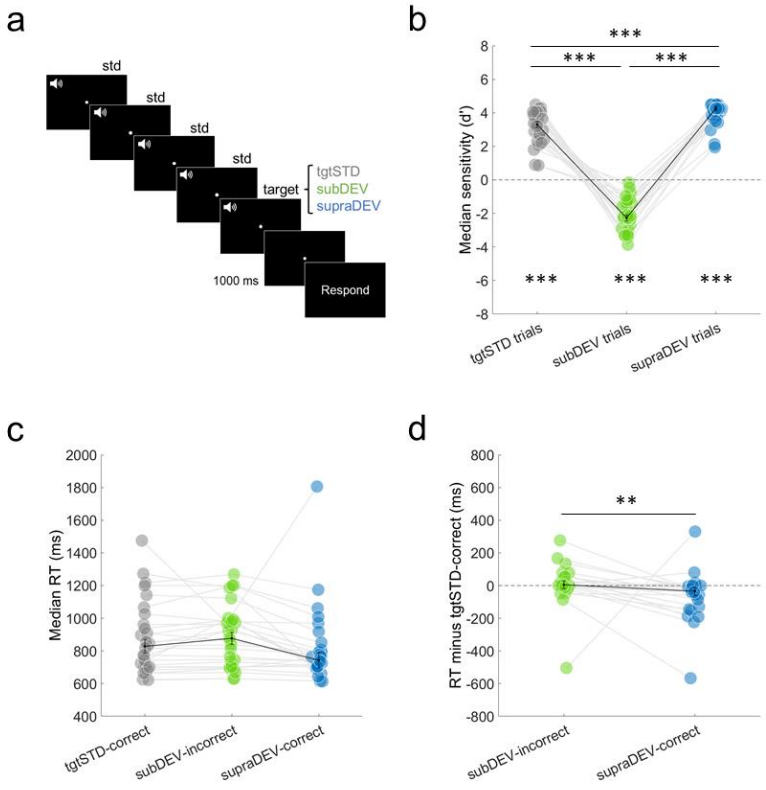

Figure 2. Main task and behavioral results. **a.** Schematic representation of a single trial. Participants had to decide whether the last of a sequence of tones was the same or

different from the preceding tones. The target could be another standard, a subthreshold or a suprathreshold stimulus. **b.** Sensitivity values for the three different types of targets. Whiskers represent the median and the standard error (S.E.) of the median. Asterisks at the bottom represent a significant difference from zero. Asterisks with bars represent a significant difference across conditions (*** < 0.001, ** < 0.01). **c.** Median reaction times for tgtSTD-correct, subDEV-incorrect, and supraDEV-correct trials. **d.** Median RT difference for subDEV-incorrect and supraDEV-correct after subtraction of tgtSTD-correct trials.

6.2. Event-related potentials

We then computed the mean ERP response to tgtSTD-correct, subDEV-incorrect, and supraDEV-correct trials (table 1 and figure 3). We focused our analyses in two different time windows: 150-250 ms and 280-380 ms, which coincide with the approximate latency of our ERP events of interest, namely the MMN and the P3. We expected to observe a more negative ERP response to both subDEV-incorrect and supraDEV-correct trials between 150-250 ms, and a positivity in the ERP wave between 280-380 ms only in response to supraDEV-correct trials. As hypothesized, a bootstrapping procedure (n = 26, one-tailed, 10,000 bootstraps, $p < 0.05$, FDR-corrected) showed that the mean ERP response recorded at electrode Cz in response to subDEV-incorrect and supraDEV-correct targets was more negative compared against tgtSTD-correct trials (figure 3a). This difference was statistically significant between ~172 and ~200 ms for subDEV-incorrect targets and between ~152 and ~192 ms for

supraDEV-correct targets. In contrast, only supraDEV-correct targets elicited a positive deflection in the ERP wave between 280 and 380.

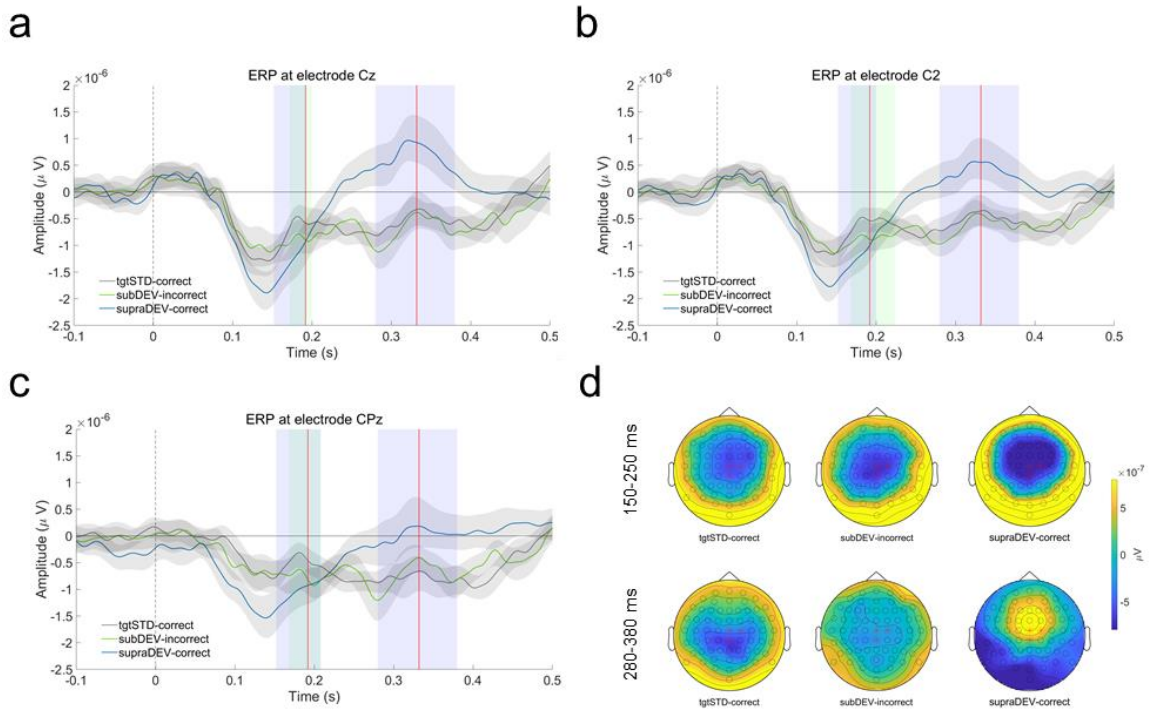

Figure 3. Event-related potentials (ERPs). Mean ERP measured at electrodes Cz (**a**), C2 (**b**) and CPz (**c**). Gray shades represent the 95% C.I. of the mean. Colored shades represent a statistically significant difference between subDEV-incorrect (green) and supraDEV-correct (blue) against tgtSTD-correct trials. **d.** Topographical maps showing ERP activation at ~192 ms (top) and ~332 ms (bottom). Latencies also indicated by red lines in time-series data. Red asterisks show location of electrodes in a, b, and c.

Similar results were observed in other centro-parietal electrodes, including C2 and CPz (figure 3b and 2c), with the amplitude of the P3 decreasing from anterior to

posterior. At ~192 ms, ERP topographies showed bilateral temporal positivities and frontal negativities consistent with scalp ERP activation associated with the MMN response (figure 3d). In turn, centro-frontal positivities at ~332 ms were also consistent with the P3 event. Early latency and fronto-central maxima suggest the observed effect is a P3a (i.e., novelty P3) response.

Component	subDEV-incorrect		supraDEV-correct	
	Amplitude (μV)	SD (μV)	Amplitude (μV)	SD(μV)
MMN	-0,874	0,766	-1,359	0,872
P3	-0,691	0,601	0,680	0,898
	minus tgtSTD-correct			
MMN	-0,322	0,851	-0,597	0,772
P3	-0,149	0,526	1,222	1,065

Table 1. Mean amplitude of ERP components at electrode Cz for subDEV-incorrect and supraDEV-correct trials, and mean difference in ERP amplitude after subtracting mean ERP responses to tgtSTD-correct trials in the time windows of statistical significance.

6.3. Source-imaging

We then studied the cortical activation dynamics associated with the processing of auditory deviance with and without conscious access using unconstrained forwards models and the sLORETA - Minimum Norm method (figure 4). In line with fMRI research on the cortical generators of the MMN and the P3 response, we expected to observe increased activation of temporal and prefrontal regions between 150-250 ms for both subDEV-incorrect and supraDEV-correct trials compared to tgtSTD-correct

trials, and increased activation of a fronto-centro-parietal network of cortical regions between 280-380 ms for supraDEV-correct trials, compared to both tgtSTD-correct and subDEV-incorrect trials. In line with our expectations, we observed increased activation of temporal and prefrontal regions for both subDEV-incorrect and supraDEV-correct compared to tgtSTD-correct trials at 190 and 225 ms after target onset (figure 4a and 3b, top rows). This difference was higher and more widespread for supraDEV-correct trials (figure 4b, top rows). At 298 and 351 ms, we observed increased activation of the most medial portion of the prefrontal cortex, and the superior aspects of the pre-central and post-central gyri for supraDEV-correct trials (figure 4b, bottom-rows). As hypothesized, no similar effect was observed for subDEV-incorrect trials (figure 4a, bottom-rows).

We also examined the extent to which the cingulate cortex is involved in the processing of auditory novelty, and how conscious access might modulate the recruitment of this cortical region. For this, we projected EEG data onto default ICBM/152 template MRIs available in the Brainstorm toolbox. We found that during early latencies (150-250 ms), both subDEV-incorrect and supraDEV-incorrect trials recruit the anterior-most portion of the cingulate, but at later latencies (> 300 ms), only supraDEV-correct targets recruit the anterior and dorsal aspect of the cingulate cortex (figure 4a and 3b, right-most column).

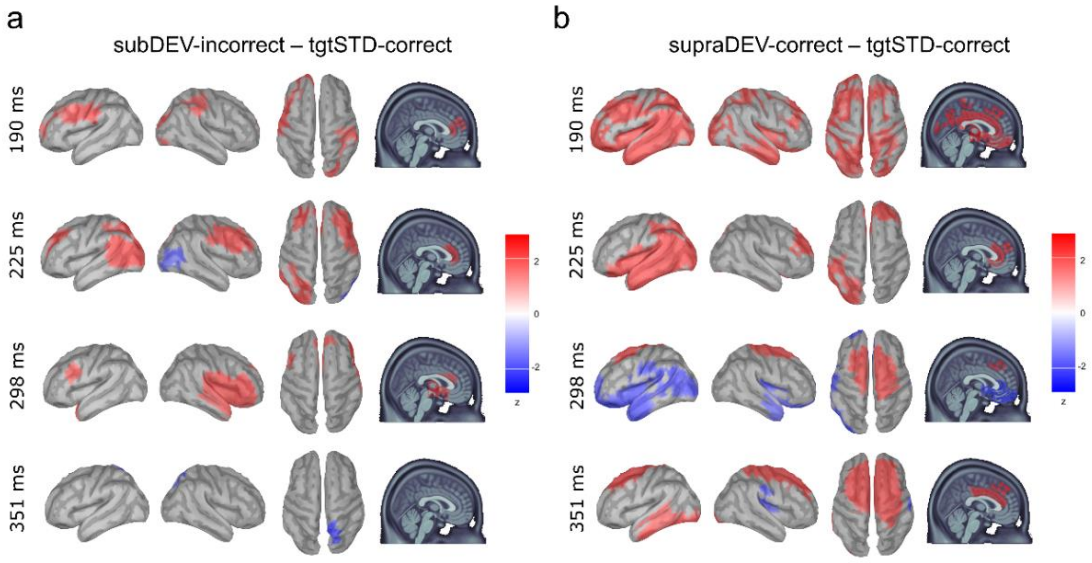

Figure 4. sLORETA source-modelling. **a.** Mean difference in cortical activation between subDEV-incorrect and tgtSTD-correct trials. Differences are represented in z units. Visualization thresholds are set at ± 2 z units. **b.** Mean difference in cortical activation between supraDEV-correct and tgtSTD-correct trials.

6.4. Pupillometry

We later investigated the evoked pupil responses to tgtSTD-correct, subDEV-incorrect, and supraDEV-correct trials. We expected to see an increase in pupil size in response to both types of trials, albeit of different amplitude, with pupil responses to supraDEV-correct trials being more pronounced than those to subDEV-incorrect trials. In sharp contrast with this expectation, results (n = 23) showed that all types of targets (including tgtSTD targets) elicited a phasic increased in pupil size, peaking at around 1,200 m after stimulus onset regardless of whether they had been consciously accessed or not (mean peak latency: tgtSTD-correct = 1110 ms, SD = 41 ms; subDEV-incorrect

= 1201 ms, SD = 33 ms; supraDEV-correct = 1203 ms, SD = 22 ms; figure 5a). The peak latency did not differ across conditions.

After subtracting the mean pupil response to tgtSTD-correct trials from the other two conditions, pupil size for subDEV-incorrect was significantly higher compared to supraDEV-correct trials between ~164 ms and ~512 ms (10,000 bootstraps, two-tailed, $p < 0.016$, figure 5b). We also studied the relationship between pupil size difference within this time window and the mean ERP values measured at electrode Cz. For supraDEV-correct trials, increased pupil sizes were associated with lower amplitude of the MMN and higher amplitude of the P3 supraDEV-correct trials within 150-250 ms (n = 22, rho = 0.43, p = 0.048, figure 5c, right) and 280-380 ms (n = 22, rho = 0.47, p = 0.027, figure 5d, right).

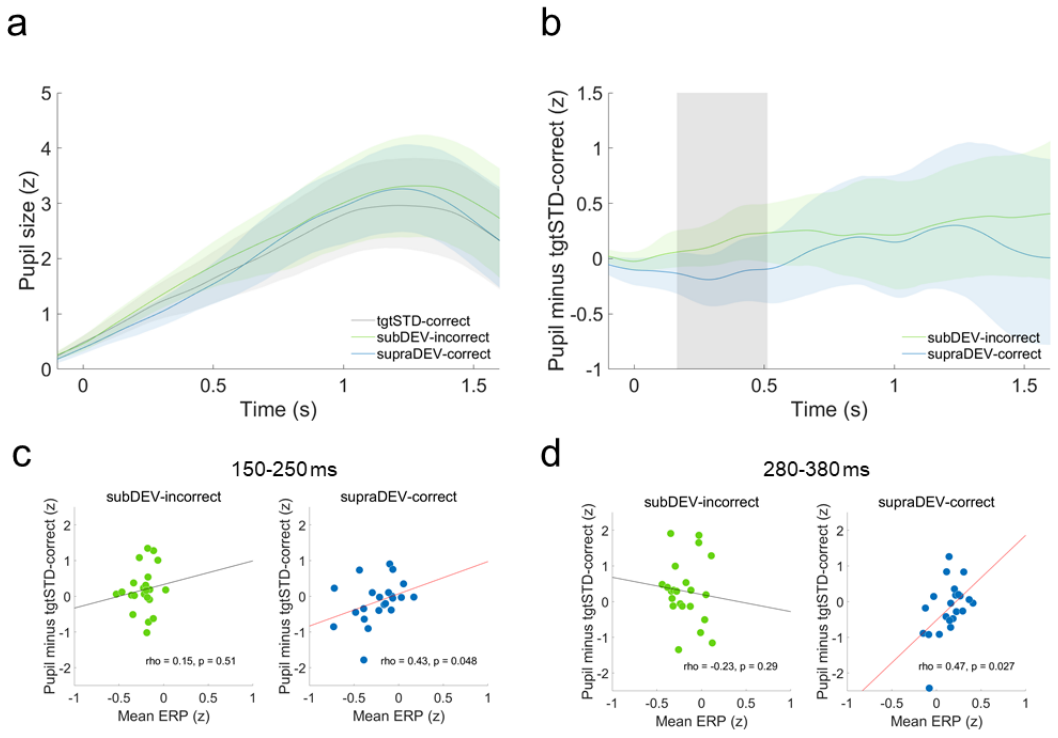

Figure 5. Pupillometry. **a.** Z-normalized mean pupil response for the three types of trials. Colored shades represent the 95% Confidence Intervals (C.I.) of the mean. **b.**

Mean pupil difference between subDEV-incorrect and supraDEV-correct trials against tgtSTD-correct trials. Gray shade represents a statistically significant difference between conditions. **c.** and **d.** Spearman correlations between mean pupil difference against tgtSTD-correct trials and mean ERP response to subDEV-incorrect and supraDEV-correct trials between 150-250 ms (**c**) and between 280-380 ms (**d**). Red best fit lines illustrate a statistically significant correlation.

6.5. Time-frequency analyses at the scalp level

Next, we studied evoked changes in theta (4-8Hz) and beta (15-30 Hz) power in response to the different types of trials (figure 6 and figure 7) by means of a non-parametric permutation test (n = 26, 10,000 permutations, two-tailed, cluster-corrected).

For theta band activity, results show that supraDEV-correct trials statistically differed from tgtSTD-correct trials between 150-250 ms in a positive cluster of centro-frontal and left temporal distribution ($t = 129.36$, $p < 0.001$), and between 280-380 ms in two positive clusters, the first of centro-frontal distribution ($t = 13.382$, $p = 0.020$) and the second of left temporal distribution ($t = 4.67$, $p = 0.034$, figure 6a). We also subtracted the mean power in response to tgtSTD-correct trials from supraDEV-correct and subDEV-incorrect trials to investigate any difference between these two conditions. Results showed that this difference was restricted to a cluster of electrodes with centro-frontal distribution, both between 150-250 ms ($t = 42.58$, $p = 0.004$) and between 280-380 ms ($t = 4.81$, $p = 0.038$, figure 6b).

Next, we estimated the average power across the electrodes contained in the biggest of these two clusters and investigated its relationship with pupil size difference. For supraDEV-correct trials only, spearman correlations (n = 23, two-tailed) showed that increased theta power is associated with decreased pupil size. This relationship was statistically significant between 150-250 ms (rho = -0.42, p = 0.046, figure 6c) and between 280 and 380 ms (rho = -0.47, p = 0.023, figure 6b).

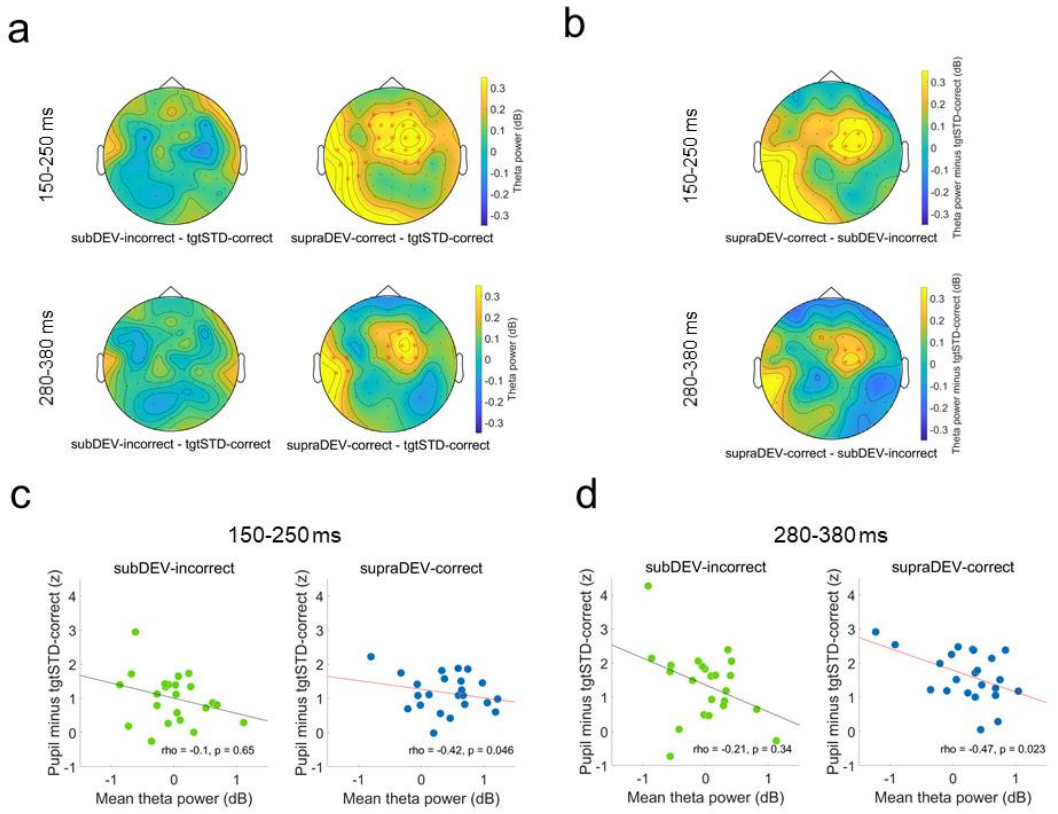

Figure 6. Wavelet time-frequency analysis in the theta frequency bands. **a.** Mean power difference between subDEV-incorrect and supraDEV-correct trials against tgtSTD-correct trials between 150-250 ms and 280-380 ms. Electrodes in red represent statistically significant clusters. **b.** Mean power difference between supraDEV-correct and subDEV-incorrect trials against tgtSTD-correct trials. **c.** and **d.** Spearman

correlation between mean pupil difference against tgtSTD-correct and mean theta power. Red lines represent a statistically significant effect.

For beta band activity, we found that supraDEV-correct trials were associated with decreased beta power compared to tgtSTD-correct trials between 280-380 ms. This effect was statistically significant for a cluster of centro-parietal and temporal distribution ($t = -86.97$, $p < 0.001$, figure 7a, bottom-right). Similarly, after subtracting the mean beta power to tgtSTD-correct trials, supraDEV-correct trials also showed a statistically significant decrease in beta power compared to subDEV-incorrect trials for a cluster of centro-parietal distribution ($t = 14.82$, $p = 0.010$, figure 7b, bottom) within the same time window. As previously done, we also examined the relationship between pupil size and beta power for the group of statistically significant electrodes in this last cluster of electrodes, but we did not find any statistically significant correlation in any of the two time-windows of interest (150-250 ms and 280-380 ms, figure 7c and 7d).

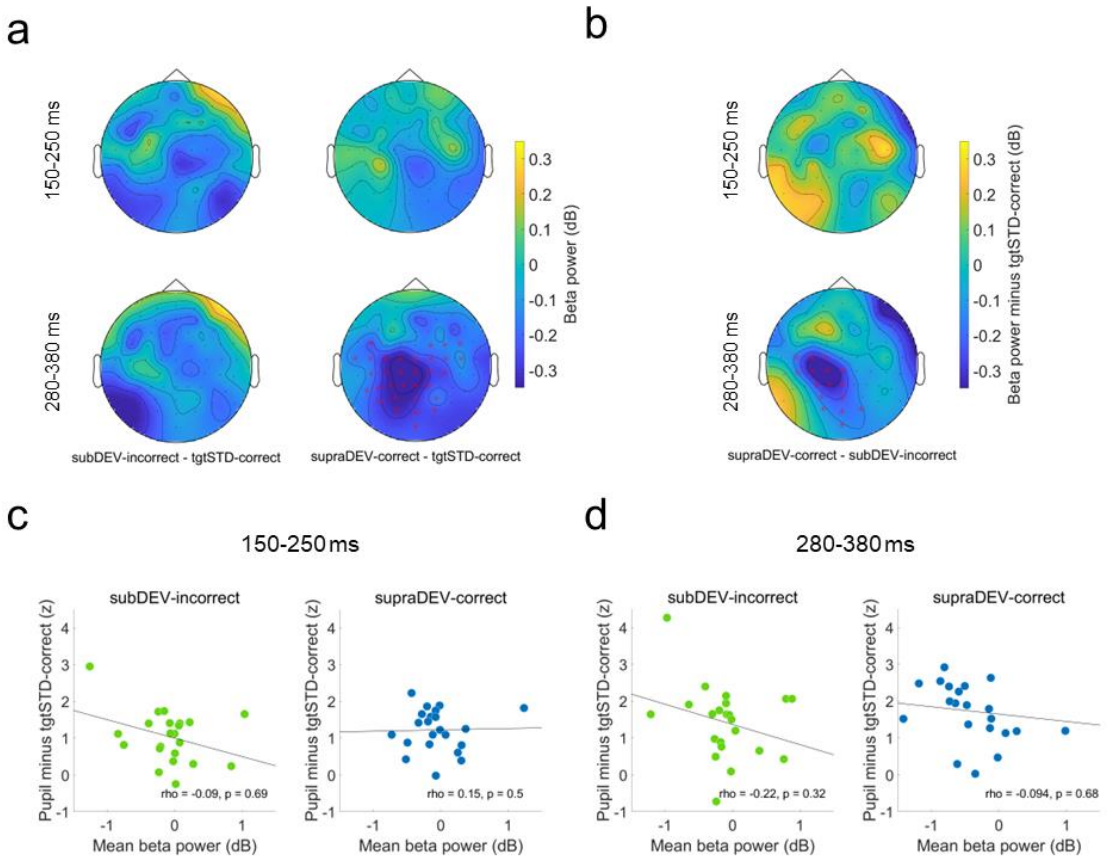

Figure 7. Wavelet time-frequency analysis in the beta frequency bands. **a.** Mean power difference between subDEV-incorrect and supraDEV-correct trials against tgtSTD-correct trials between 150-250 ms and 280-380 ms. Electrodes in red represent statistically significant clusters. **b.** Mean power difference between supraDEV-correct and subDEV-incorrect trials against tgtSTD-correct trials. **c.** and **d.** Spearman correlation between mean pupil difference against tgtSTD-correct and mean theta power. Red lines represent a statistically significant effect.

6.6. Time-frequency analyses in source reconstructed space

We then investigated brain oscillatory dynamics at the source level. For this, we performed a wavelet time-frequency decomposition across the 100 parcellations in the 7-network Schaefer's functional atlas. Consistent with previous M/EEG studies, we expected to see theta (4-8 Hz) in temporal regions and beta (15-30 Hz) power increases prefrontal.

In partial agreement with this hypothesis, a cluster-corrected permutation procedure showed a sustained increase in theta power for subDEV-incorrect trials in left posterior middle and superior temporal gyrus (pM/STG) between approximately 350 and 1,500 ms (10,000 permutations, one-tailed, $p < 0.05$, figure 8a), and a transient increase in beta power in the left OFC between ~ 450 and 550 ms (10,000 permutations, one-tailed, $p < 0.05$, figure 8a). For supraDEV-correct trials, we observed sustained, time-locked increases in theta power in the right temporal pole (0-100 ms) and the somatomotor portion of the left posterior insula and Heschl's gyrus (pINS/HG, 0-600 ms, 10,000 permutations, one-tailed, $p < 0.05$, figure 8b, top rows). In turn, we observed transient increases in increases in beta power in the left ACC between 450 and 550 ms, and in the right posterior cingulate cortex (PCC) between approximately 600 and 700 ms (10,000 permutations, one-tailed, $p < 0.05$, figure 8b, bottom rows). Interestingly, for this latter region, we also observed a sustained increase in alpha power between 400 and 1,000 ms.

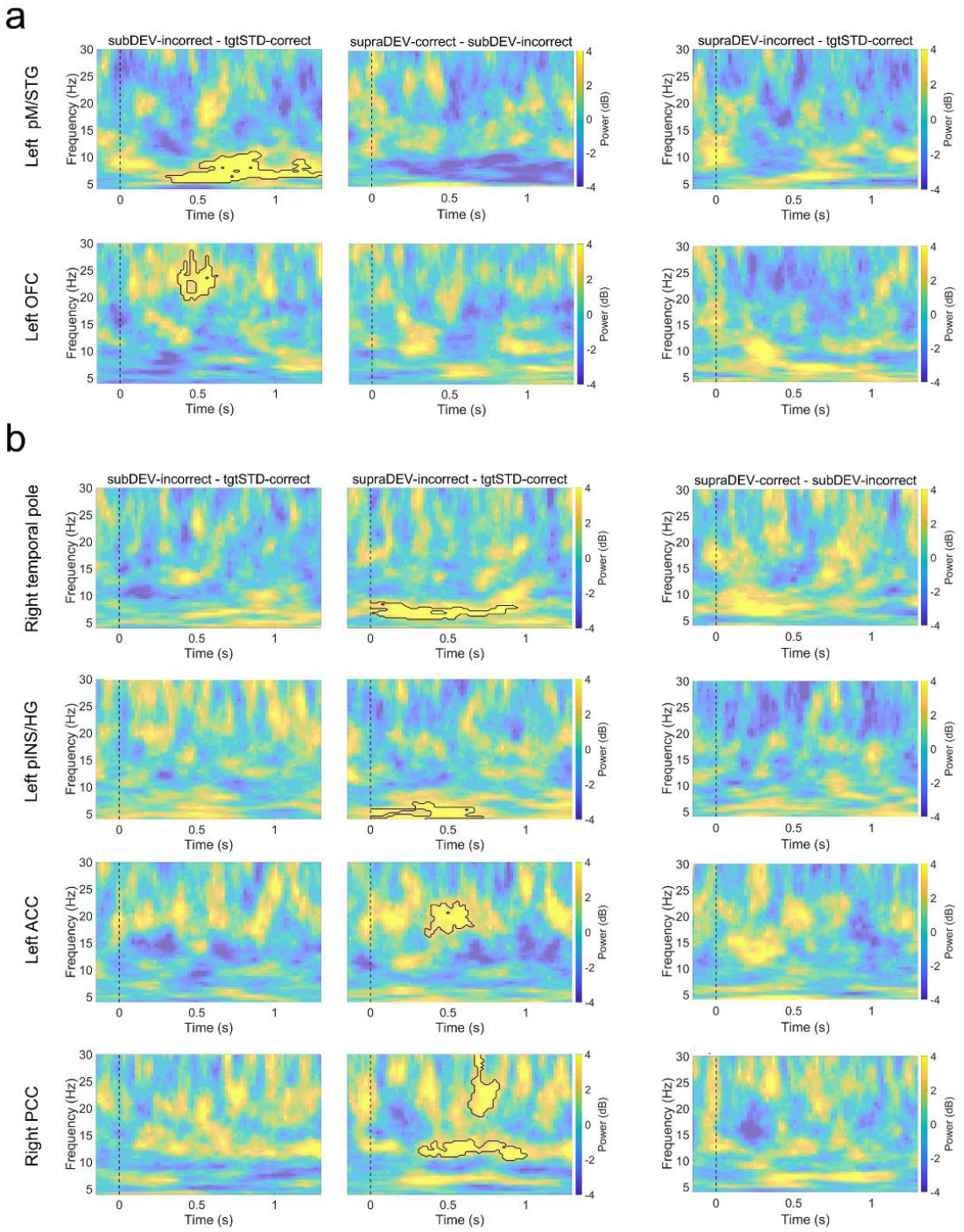

Figure 8. Wavelet time-frequency analyses in source reconstructed signals. **a.** Theta and beta power increases for subDEV-incorrect trials compared to tgtSTD-correct trials, and mean difference between supraDEV-correct and subDEV-incorrect trials

after subtracting tgtSTD-correct (right-most colums). Black contours show a statistically significant effect ($p < 0.05$, cluster-corrected, one-tailed). **b.** As in a but for supraDEV-correct trials.

We also sought to understand how theta and beta power increases at the source level would relate to phasic increases in pupil size in our two time-windows of interest. Spearman correlation analyses (n = 23, two-tailed) showed that the mean pupil size difference and mean theta power are negatively correlated in the left ACC for subDEV-incorrect trials (rho = -.48, p = 0.023, uncorrected, figure 9a) and in the right temporal pole for supraDEV-correct trials (rho = -0.46, p = 0.028, two-tailed, figure 9c) between 280 and 380 ms. In turn, an increased pupil size difference is associated to increased theta power in the left pINS/HG for both subDEV-incorrect (rho = 0.46, p = 0.03, uncorrected) and supraDEV-correct trials (rho = 0.46, p = 0.027, uncorrected) between 150 and 250 ms (figure 9b). Finally, between 280-380 ms, a higher mean pupil size difference was associated to decreased beta power in the right PCC (rho = -0.58, p = 0.004, uncorrected, figure 9d). We found a positive association between pupil size difference and beta power in the left OFC for subDEV-incorrect trials, yet this effect did not reach significance (n = 23, rho = 0.41, p = 0.053, uncorrected, annex 5)

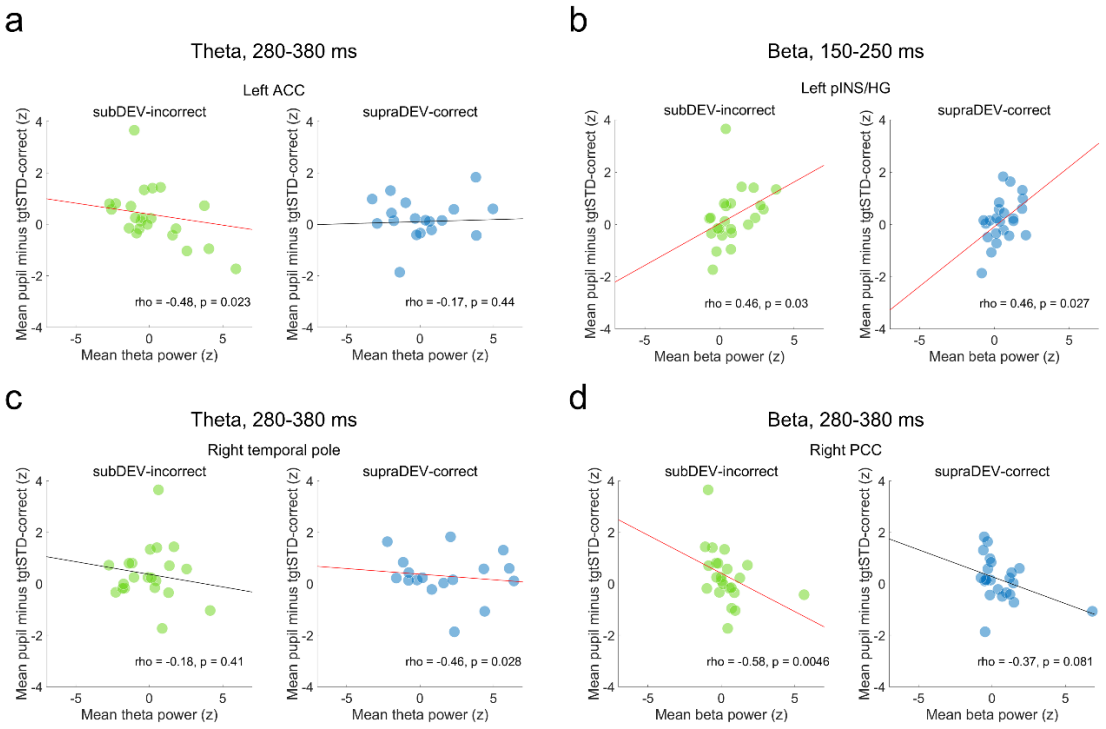

Figure 9. Correlations between mean pupil size difference and mean theta/beta power at the source level at **a.** left ACC between 280-380 ms, **b.** left pINS/HG between 150-250 ms, **c.** right temporal pole between 280-380 ms, and **d.** right PCC between 280-380 ms. Red lines represent a statistically significant effect.

6.7. Functional connectivity

Finally, we studied functional connectivity (FC) patterns between temporal, prefrontal and cingulate regions using source-reconstructed time-frequency data in two separate time windows: 0-250 ms and 250-500ms (n = 26, two-tailed, figure 10). We expected increased FC in the theta (4-8 Hz) frequency range during conscious processing of auditory deviance, and increased FC in the range of beta (15-30 Hz)

during subconscious processing of auditory deviance. Our results only lend partial support to this hypothesis.

6.7.1. Theta-band functional connectivity

Between 0-250 ms, only fronto-temporal FC for supraDEV-correct ($t = 4.33$, $SD = 0.012$, $p = 0.002$, FDR-corrected, figure 10a, top-left) statistically differed from zero. When compared to subDEV-incorrect trials, theta-band fronto-temporal FC for supraDEV-correct trials was statistically higher ($t = 3.80$, $SD = 0.020$, $p = 0.005$, FDR-corrected, figure 10a, top-left). Between 250-500 ms, cingulo-temporal FC ($t = 4.99$, $SD = 0.017$, $p < 0.001$, FDR-corrected, figure 10a, bottom-left) and fronto-cingular FC ($t = 304$, $SD = 0.024$, $p = 0.032$, FDR-corrected, figure 10a, bottom-middle) for supraDEV-correct trials was significantly higher than zero. When compared against subDEV-incorrect trials, fronto-cingular ($t = 2.99$, $SD = 0.037$, $p = 0.037$, FDR-corrected, figure 10a, bottom-middle) and fronto-temporal FC ($t = 2.09$, $SD = 0.030$, $p = 0.046$, uncorrected, figure 10a, bottom-right) were statistically higher in the theta frequency range.

6.7.2. Beta-band functional connectivity

Between 0 and 250 ms, fronto-cingular ($t = -2.07$, $SD = 1.55$, $p = 0.049$, uncorrected, figure 10b, top-middle) and fronto-temporal FC ($t = 3.07$, $SD = 0.009$, $p = 0.043$, FDR-corrected, figure 10b, top-right) statistically differed from zero. When compared across conditions, fronto-cingular FC for subDEV-incorrect trials was statistically higher than FC for supraDEV-correct trials ($t = 2.39$, $SD = 0.015$, $p = 0.025$,

uncorrected, figure 10b, top-middle), whereas fronto-temporal FC was statistically higher for supraDEV-correct trials compared against subDEV-incorrect trials ($t = 2.92$, $SD = 0.012$, $p = 0.044$, FDR-corrected, figure 10b, top-right). Between 250-500 ms, fronto-cingular ($t = 4.55$, $SD = 0.015$, $p < 0.001$, FDR-corrected, figure 10b, bottom-middle) and fronto-temporal FC ($t = 5.83$, $SD = 0.008$, $p < 0.001$, FDR-corrected, figure 10b, bottom-right) for supraDEV-correct trials statistically differed from zero. When compared against subDEV-incorrect trials, beta-band fronto-cingular ($t = 3.48$, $SD = 0.019$, $p = 0.005$, FDR-corrected, figure 10b, bottom-middle) and fronto-temporal FC ($t = 4.69$, $SD = 0.013$, $p < 0.001$, FDR-corrected, figure 10b, bottom-right) were statistically higher.

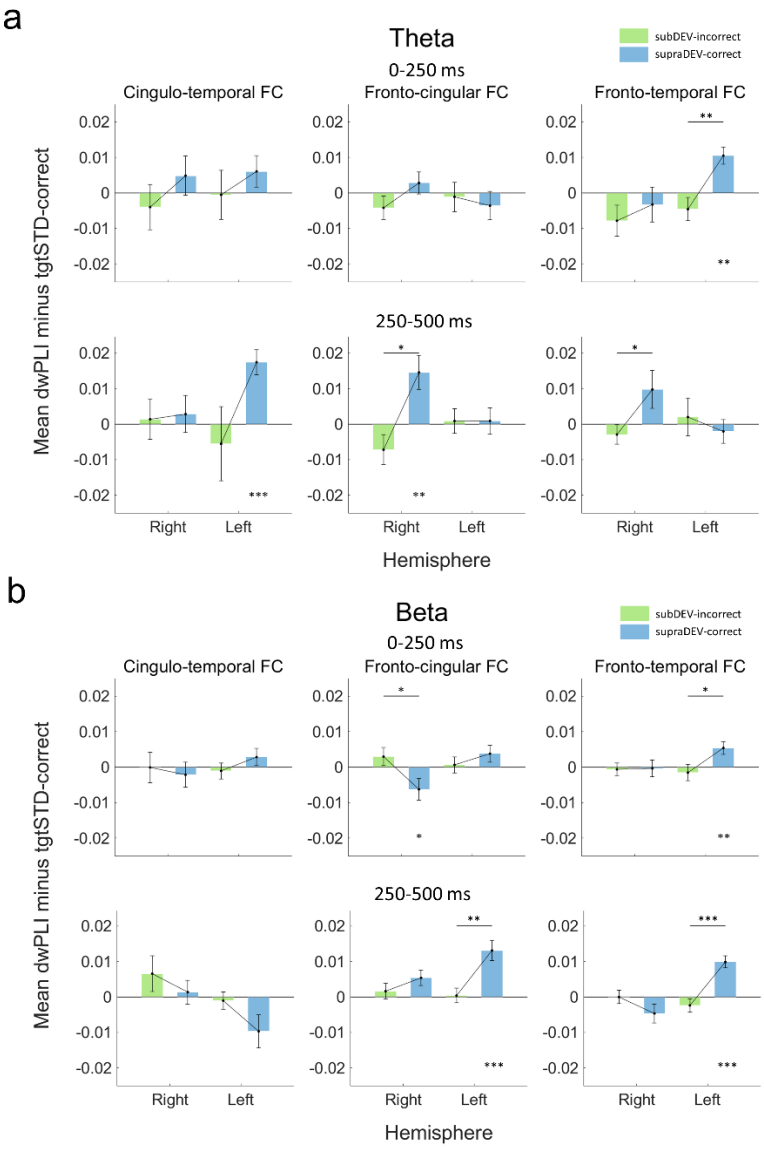

Figure 10. Functional connectivity analyses. **a.** mean debiased wPLI difference for subDEV-incorrect (green bars) and supraDEV-correct (blue bars) trials against tgtSTD-correct trials within the range of theta oscillations. **b.** Same as in a, but beta-band FC. Asterisks at the bottom of each panel represent a statistically significant difference from zero. Whiskers show the standard error of the mean. Lines and asterisks on top represent a statistically significant difference across conditions (* $p < 0.05$, ** $p < 0.01$, *** $p < 0.001$).

7. Discussion

7.1. Behavioral and electrophysiological validation of our experimental design

In this study, we investigated how the brain responds to auditory deviance with and without conscious access. Our first objective was to design a paradigm that allowed disentangling conscious from subconscious processing of auditory deviance. To this end, we combined an auditory staircase procedure with a modified version of the classical auditory oddball task. We presented to participants sequences of tonal stimuli of variable length, where the last stimulus could be another standard tone, a subthreshold target, or a suprathreshold target. Participants were asked to report whether the last stimulus in each sequence was the same or different from the preceding ones.

Results show that subDEV targets were systematically and correctly reported as standard tones (figure 2b). We take this as evidence that such trials reflect subconscious processing but not conscious access to auditory deviance. On the other hand, systematic and correct identification of supraDEV targets reflects conscious access to auditory deviance (figure 2b). By subtracting reaction time to target standards from these two conditions, we could establish that subDEV stimuli were responded to more slowly, whereas supraDEV targets were responded to faster, compared to tgtSTD-correct trials (figure 2c). This suggests that decision making processes were sped up when the deviant was consciously accessed and delayed when it subconsciously processed, which is in line with evidence showing how saliency and

uncertainty facilitate and hamper behavioral responses during goal directed behavior, correspondingly (Garcia et al., 2017; Kayser et al., 2005; Perugini et al., 2016; Teixeira et al., 2014).

Our second objective was to replicate previous findings from the ERP literature showing that the MMN and the P3 are reliable markers of subconscious and conscious processing of auditory deviance. Subconscious processing of auditory deviance is indexed by the MMN negativity, a response that reflects the automatic generation of sensory memory traces and detection of mismatching representations in early auditory cortices, which is independent of conscious access (Bekinschtein et al., 2009; Fischer et al., 1999; Garrido et al., 2009; Näätänen et al., 2007, 2011; Tiitinen et al., 1994). In turn, conscious access to deviance is associated with the P3, an event that reflects context updating, information maintenance and memory-dependent decision making processes (Comerchero & Polich, 1999; Nieuwenhuis et al., 2005; Polich, 1987, 2007; Ranganath & Rainer, 2003; Sutton et al., 1965). We successfully replicated these findings by showing that both subthreshold and suprathreshold deviants elicit a MMN response at around ~200 ms, regardless of whether they were consciously accessed as deviants or not (figure 3a). However, only consciously accessed subthreshold targets were associated with a fronto-central positivity in the ERP wave between 280 and 380 ms (figure 3a and 3d), consistent with the temporal and spatial characteristics of the P3 event (Comerchero & Polich, 1999; Escera & Malmierca, 2014; Ranganath & Rainer, 2003), and more specifically, the P3a subcomponent of the P3 response complex. Since the P3a is usually observed in response to non-target deviants in three-stimulus oddball tasks, we expected to observe a P3b rather than a P3a, which is more

frequently observed in response to an attended and consciously reported novel stimulus. Because participants were instructed to withhold their response for 1,000 ms, the absence of a P3b response in our task could be explained by a trial-to-trial jitter in decision-making processes and overt motor responses, which presumably underlie this later subcomponent. Nevertheless, the P3a also reflects the conscious identification of above-threshold auditory irregularities and consequently can be taken to reflect early information-processing stages during conscious access to auditory deviance.

Taken together, our behavioral and electrophysiological data validate our experimental design. Suprathreshold targets triggered a series of neural events characteristic of information broadcasting to higher-order neural processors, indexed by the P3, whereas subthreshold targets elicited local processing signals indexed by the MMN. This implies that our task successfully teased apart subconscious processing from conscious access to sensory deviance in the auditory domain, as intended by our objective number one, and allowed us to replicate well-established findings on the markers of conscious and subconscious processing of auditory deviance, as intended with objective number two.

7.2. EGG source modelling reveals cortical activation dynamics consistent with MMN and P3 generators

Our third objective was to stablish the cortical activation dynamics associated with the processing of auditory deviance with and without conscious access. We employed EEG source-imaging methods to investigate whether cortical activation dynamics observed during our task were consistent with the known cortical generators

of the MMN and P3, as previously reported in fMRI research (Garrido et al., 2009; Hyman et al., 2017; Li et al., 2009; Linden, 2005; Polich, 1987).

Our results stand in line with the known origins of these neural events: for subDEV-incorrect targets, we found increased activation of temporal regions bilaterally, and right central and prefrontal regions between approximately 180 and 225 ms, compared to tgtSTD-correct trials (figure 4a). For supraDEV-correct trials, we found widespread and sustained activation of temporal regions and prefrontal regions bilaterally within the same time window (figure 4b). Bilateral temporal and right prefrontal activation at around 200 ms after target onset are both hallmarks of the MMN response (Garrido et al., 2009; Näätänen et al., 2007, 2011; Tiitinen et al., 1994). The recruitment of these regions presumably reflects early sensory memory processes that sustain automatic predictive mechanisms, as well as the involvement of ventral attention and saliency networks located in prefrontal cortical regions (Garrido et al., 2009; Kompus et al., 2020).

From 330 ms onwards, EEG source-imaging analyses show the widespread activation of a fronto-centro-parietal network during the processing of supraDEV-correct trials, which is also consistent with the known cortical generators of the P3 response (figure 4b, bottom panels). Activation within these regions indexes the joint contribution of the dorsomedial prefrontal cortex, supplementary motor areas, somatomotor regions, and superior parietal association cortices during controlled processing and conscious access to a novel sensory stimulus (Comerchero & Polich, 1999; Linden, 2005; Polich, 1987). Our results also suggest a fronto-central activation maxima during this neural event, thus providing further evidence that the observed

response is a P3a (or novelty P3), rather than a P3b. This, paired with the recruitment of the anterior cingulate cortex, a region known to code stimulus saliency, suggests that the observed response reflects the conscious evaluation of a deviant sensory stimulus prior to subsequent decision-making processes and overt behavioral responses.

Some studies have proposed a central role of the cingulate cortex in the processing of auditory deviance (Kim et al., 2020; Li et al., 2009). In line with these studies, we found that cingulate regions were recruited in latencies consistent with both the MMN and the P3 (figure 4a and 4b). However, while the cingulate is involved at around 200 ms across conditions, the most dorsal aspect of the ACC is recruited only during processing of supraDEV-correct targets in a latency consistent with the P3 response. These latter results show a multifaceted role of the cingulate cortex: generalized activation of anterior and posterior aspects of the cingulate at around 200 ms suggests a role in bottom-up sensory processing, presumably through automatic attentional capture and reorientation, independently of stimulus identity or conscious access. Subsequently, the specific involvement of this same region in its most dorsomedial portion in in a latency that matches the peak of the P3 component is consistent with a proposed role of the dorsal ACC in gating perception and conscious access during goal-directed behavior (Aston-Jones & Cohen, 2005; Benedict & Lockwood, 2002; Nieuwenhuis et al., 2005; Orr & Weissman, 2009).

7.3. Pupil size encodes behavioral relevance and sensory uncertainty

Our fourth objective was to identify the pupillary dynamics associated with the processing of auditory deviance with and without conscious access. Some studies

suggest that the pupil reflects conscious access to sensory deviance and regularity violations (Bala et al., 2020; Quirins et al., 2018), whereas others indicate that the pupil is sensitive to task-specific behavioral demands (Liao et al., 2016; Zhao et al., 2019). Our results align with the latter line of evidence. All targets elicited a phasic increase in pupil size that peaked at around 1,200 ms, regardless of stimulus identity or whether they were consciously accessed as deviant or not (figure 5a). This confirms that the that the pupil the attentional reallocation mechanisms and overt decision-making processes in response to behaviorally-relevant stimuli (Liao et al., 2016; Zhao et al., 2019). Additionally, we observed increased pupil size difference to subthreshold targets within an earlier time window (~164-512 ms, figure 4b). This suggests that the phasic pupil response also reflects unexpected uncertainty during sensory scene analysis, which is in line with an extensive line of work on how uncertainty modulates pupil responses in perceptual, attentional and learning tasks (Alamia et al., 2019; Urai et al., 2017; Zhao et al., 2019).

Our findings, on the other hand, provide no evidence whatsoever that the pupil response can be considered a reliable marker of conscious access to auditory deviance. Instead, they fit well with the idea that phasic discharges of the neuromodulator NE regulate global arousal levels during adaptive and goal-directed behavior (Aston-Jones & Cohen, 2005; Cockburn et al., 2021; Vazey et al., 2018). We therefore propose that the phasic pupil responses observed in our task reflects the contribution of two separate components: a component that indexes arousal adaptation driven by unexpected sensory uncertainty and another component reflecting stimulus-driven attentional capture by a behaviorally relevant stimulus. This highlights a variegated involvement

of pupil-linked mechanisms in different stages of neural information processing and is in line with recent evident that pupil responses can account for different aspects of attention, including orienting, alerting and cognitive control (Strauch et al., 2022). Importantly, we also found a positive association between pupil size difference and the P3 response for consciously accessed auditory deviant stimuli (figure 5d). This fits evidence from studies in animal models showing that both P3 and pupil responses are sensitive to NE modulation (Aston-Jones & Cohen, 2005; Masson & Bidet-Caulet, 2019; Nieuwenhuis et al., 2005). In contrast, increased pupil size difference is associated with decreased amplitude of the MMN. This is in line with previous work showing that MMN amplitude scales linearly with contrast-based saliency (Sams et al., 1985; Tiitinen et al., 1994), whereas pupil responses increase with higher uncertainty (Alamia et al., 2019; Lavín et al., 2014; Urai et al., 2017). We therefore propose that this negative relationship reflects the opposite nature of the uncertainty-driven component of the pupil response and the saliency-driven, error-detection mechanisms indexed by the MMN.

		Behavior	ERP	Pupil response
Conscious processing	Effect	Faster reaction times High accuracy rates	MMN and P3	Decreased early pupil response and late peak
	Cognitive interpretation	Response facilitation due to increased stimulus saliency	Local detection of mismatching representations and information broadcasting to orienting attention and saliency processors	Current arousal levels are enough to meet task demands Attentional reallocation to behaviorally relevant stimuli
Subconscious processing	Effect	Slower reaction times High error rates	MMN	Increased early pupil response and late peak
	Cognitive interpretation	Response hampering due to increased sensory uncertainty	Local detection of mismatching representation without information broadcasting to orienting attention and saliency processors	Arousal adaptation due to heightened uncertainty Attentional reallocation to behaviorally relevant stimuli

Table 2. Summary of behavioral, ERP analyses and pupillometric results.

7.4. Oscillatory dynamics in response to auditory deviance with and without conscious access

As our fifth objective, we wanted to identify the oscillatory dynamics that underlie the processing of auditory deviance with and without conscious access. In line with previous studies (El Karoui et al., 2015; Javitt et al., 2017; Rescaens et al., 2018), we had hypothesized that conscious processing of deviance would be characterized by increased theta band power in temporal regions whereas subconscious processing of auditory deviance would be associated with increased beta power in prefrontal regions. Although scalp time-frequency results lend partial support to these expectations, our source-space results also suggest a more complex and dynamic scenario than initially

hypothesized, as effects in both frequencies were observed during conscious and subconscious processing of novelty at the source level.

7.4.1. Increased theta power reflects information-maintenance and processing effort

Increases in theta power have been observed following the detection of deviant auditory stimuli in time windows that are consistent with the latencies of the MMN and the P3a ERP events (Hsiao et al., 2009; Javitt et al., 2018; Recasens et al., 2018; Solís-Vivanco et al., 2021). In line with these studies, we found that conscious access to deviance is related to increased theta power between 150-250 and 280-380 ms at the scalp level (figure 6a). Moreover, our results show that this occurs only when novelty is consciously accessed. This is compatible with a proposed role of theta oscillations in supporting conscious states and perception via attentional sampling, memory-based computations and information integration (Haque et al., 2020; Klimesch et al., 2001; Slagter et al., 2009).

At source level, we expected to observe increased theta power in temporal regions for consciously accessed deviant stimuli only. In contrast with this expectation, we found increases in theta power in different temporal regions for both consciously and subconsciously processed deviants. Subconsciously processed deviant stimuli were associated with increases in theta power in the posterior aspect of the M/STG (figure 7a), whereas consciously accessed deviant stimuli were associated to theta power increases in the right temporal pole and left pINS/HG (figure 7b). Generally speaking, these results are in line with previous studies which suggest theta oscillations

reflect the detection of violations to self-generated auditory predictions (Haque et al., 2020; Hsiao et al., 2009; Javitt et al., 2018; Solís-Vivanco et al., 2021). However, our results also extend these findings by showing how conscious and subconscious processing of deviance elicits theta power increases in different parcellations of the temporal lobe.

We believe that theta power increases in the pM/STG for subconsciously processed deviant stimuli reflects increased effort or processing load due to heightened sensory uncertainty, whereas increases in the pINS/HG and the temporal pole for consciously accessed deviant stimuli reflect suprathreshold stimulus information maintenance, which is readily available for global broadcasting to prefrontal or anterior temporal processors. The latter claim is supported by neuroanatomical evidence showing that the temporal pole, which is already a multimodal hub where complex information processing takes place, has intricate connections to several subdivisions of the PFC, underscoring a potential role of this cortical regions in bridging sensory processing and higher order cognitive processes (Córcoles-Parada et al., 2019).

Finally, increased theta power observed at the scalp level (figure 6a), and in left ACC (figure 9a) and the right temporal pole (figure 9c) was associated with a decreased pupil size. This finding further confirms that theta power and pupil responses reflect sharply different cognitive processes, with the former presumably involved in information-maintenance during sensory unambiguous events and latter at least partially reflecting sensory uncertainty during auditory scene analysis.

7.4.2. Beta oscillations reflect sensory uncertainty and prediction error

We found that conscious access to novelty was associated to decreased beta (15-30 Hz) band power compared to tgtSTD-correct and to subDEV-incorrect targets (figure 7a and 7b). This is in line with El Karoui et al. (2015), who found that global violations of statistical regularities in long auditory sequences are associated with a power decrease in the beta (13-25 Hz) frequency band starting at around 250 ms. However, our results stand at odds with those of Chang et al. (2016), who found that unpredictable pitch change in auditory sequences results in a power increase in the beta frequency band (15-20 Hz) between 200-300 ms after odd stimulus onset. Beta oscillations have been previously associated with feedback signaling and top-down modulation, as well as to error-detection mechanisms upon detection of violations to temporal predictions (Arnal et al., 2015; Chang et al., 2016; El Karoui et al., 2015; Miller et al., 2018). Because our results show that increased beta power are associated with subconscious processing of novelty, rather than with conscious access, it could therefore be that such increase in beta power is signaling top-down modulation resulting from increased sensory uncertainty. If this was the case, we would also expect a positive relationship between pupil size and beta power. However, correlation analyses showed no evidence of such effect between 150-250 ms or between 280-380 ms. Finally, we did find some evidence of increase beta power for consciously accessed novelty between 150-250 ms (figure 7b, top), which would confirm a role of beta in conscious detection of violations to temporal predictions, this effect was also not statistically significant.

Source-reconstructed signals show beta power increases in the left ACC, right PCC, and the OFC (figure 8a and 8b). This is interesting because all of these cortical regions have been previously proposed to make part of a cortico-subcortical noradrenergic-mediated network in charge of regulating arousal levels during adaptive and goal-directed behavior (Aston-Jones & Cohen, 2005; Nieuwenhuis et al., 2005; Vazey et al., 2018). In turn, beta oscillations have been proposed as the carriers of feedback information and top-down modulatory signals in the neocortex (Bastos et al., 2018; Miller et al., 2018; Richter et al., 2017, 2018).

Subconscious processing, but not conscious access to auditory deviance, was associated with increased beta power in the left OFC (figure 8a). Research in non-human primates and rodents has shown vast descending and ascending projections from the OFC and other frontal regions to the Locus Coeruleus, the main noradrenergic nucleus in the brainstem (Arnsten & Goldman-Rakic, 1984; Chandler et al., 2014). Additionally, increased beta-band activity has been previously proposed to reflect response uncertainty (Tzagarakis et al., 2010) and stimulus uncertainty (Chang et al., 2016). We therefore propose that beta oscillations in the OFC reflect uncertainty-driven top-down modulation targeting subcortical nuclei and signaling the need for phasic arousal adaptation via phasic liberation of norepinephrine. Although it did not reach significance, we observed a positive association between pupil size and beta power in this region for subconsciously processed deviant stimuli ($rho = 0.41$, $p = 0.053$, annex 5), which lends some support to this idea. Although thought-provoking, however, such claim begs further research. Moreover, others have previously reported an involvement of parietal regions in encoding uncertainty (Horan et al., 2019; Zhong et al., 2019). We,

however, did not find any statistically significant increase in beta power in parietal areas. in response to auditory deviance with or without conscious access. This means that uncertainty-mediated parietal responses might be related to higher-order uncertainty processing (i.e., response uncertainty), rather than perceptual uncertainty.

Conscious processing of auditory deviance was also associated with increased beta power in the left ACC and the right PCC (figure 8b). The left ACC makes part of the saliency network and is implicated in gating orienting attention responses during detection of novel sensory stimuli (Dehaene et al., 1998; Orr & Weissman, 2009). Beta power increases in this region could therefore reflect error detection mechanisms, as others have previously suggested (Hyman et al., 2017). This response would be stimulus-driven and attention-dependent, similarly (or relatedly) to the P3a event, which is in line with evidence of ACC contribution to this ERP event (Nieuwenhuis et al., 2005; Orr & Weissman, 2009; Polich, 2007). Later increases in beta power in PCC (~700 ms) might in turn reflect subsequent information integration and, ultimately, decision-making processes, which is in line with previous work on the contribution of the PCC to these cognitive mechanisms (Akaishi et al., 2014; Joshi et al., 2016; Pearson et al., 2011).

Notably, we found a positive correlation between mean beta power and mean pupil difference across conditions in the left pINS/HG (figure 9b). We suggest that this effect, which is independent of stimulus identity or conscious access, reflects the involvement of this region in encoding temporal and auditory predictions (El Karoui et al., 2015). In turn, a negative association between pupil size and beta power in the PCC for consciously processed deviant stimuli (figure 9d) suggests that this region's

contribution to error-detection processes crucially depends on conscious access to sensory prediction violations.

7.5. Functional connectivity

Our last objective was to identify the patterns of functional connectivity that characterize the processing of auditory deviance with and without conscious access. For this, we estimated functional connectivity (FC) between cingulate and temporal regions (cingulo-temporal FC), between prefrontal and cingulate regions (fronto-cingular FC), and between frontal and temporal regions (fronto-temporal FC). We had hypothesized that conscious perception of auditory deviance should be associated to increased FC between these regions in the theta (4-8 Hz) frequency range, whereas subconscious perception of auditory deviance should be associated with increased FC in the beta (15-30 Hz) frequency range. Except for cingulo-temporal FC, our results do not lend strong support to this functional division for theta and beta band functional connectivity.

7.5.1. Theta-band FC supports conscious access to novelty through stimulus and saliency information broadcasting

For consciously accessed deviant stimuli, we found evidence of statistically significant increases left-hemisphere fronto-temporal FC between 0 and 250 ms (figure 10a, top row), and in right-hemisphere fronto-cingular and fronto-temporal FC between 250 and 500 ms (figure 10a, bottom row). Generally speaking, these findings are in line with previous evidence that theta oscillatory mechanisms support conscious

perception of sensory events (Haque et al., 2020; Klimesch et al., 2001; Slagter et al., 2009). More specifically, we suggest that increased fronto-temporal FC during conscious processing of deviance reflects information exchange about deviant stimulus identity between auditory mechanisms involved in early automatic error detection mechanisms and orienting attention mechanisms in prefrontal regions. In turn, increased theta-band fronto-cingular FC during conscious access to deviance would reflect information exchange between cortical processors encoding stimulus saliency and decision-making processes in cingulate regions and prefrontal regions. Such global information exchange is indeed a hallmark of access consciousness, as previously elaborated (Dehaene et al., 1998, 2006; Mashour et al., 2020; Naccache, 2018)

7.5.2. Beta-band FC signals subconscious uncertainty and conscious error detection

Beta-band FC connectivity results only partially align with our expectations. For subconscious processing of deviance, we only found evidence of increased beta-band FC between frontal and cingulate regions in the early time window between target onset and 250 ms (figure 10b, top-middle). We suggest that, considering such early latency, and unlike parietal regions which reflect higher order uncertainty (Horan et al., 2019; Zhong et al., 2019), increased beta-band fronto-cingular FC reflects top-down mechanisms signaling the need of adapting arousal levels due to increased perceptual uncertainty. In support of this view, previous studies implicate these regions, which feature dense bidirectional anatomical connections, in a NE-mediated circuit involved in arousal adaptation through a modulation of cortical excitation-inhibition balances

(Aston-Jones & Cohen, 2005; Jodo et al., 1998; Joshi et al., 2016; Nieuwenhuis et al., 2005; Orr & Weissman, 2009). This mechanism would therefore operate independently of conscious control and would contribute to lowering perceptual thresholds to meet task demands in subsequent trials. However, this idea is only tentative and would require further research.

In contrast, we found evidence of increased beta-band fronto-temporal FC for consciously accessed deviance between 0 and 250 ms (figure 10b, top-right), and increased beta-band fronto-cingular (figure 10b, bottom-middle) and fronto-temporal FC (figure 10b, bottom-right) between 250 and 500 ms. We propose that these results reflect information exchange about a consciously detected prediction error between temporal areas in charge of early sensory memory and involved in automatic error detection, prefrontal regions in charge of saliency-driven stimulus evaluation and cingulate regions involved in decision making. This is in line with evidence showing that beta oscillations reflect top-down modulation following prediction errors, which presumably signal the need to update internally generated models during sensory scene analysis (Aston-Jones & Cohen, 2005; Chang et al., 2016; Tzagarakis et al., 2010).

		θ power	β power	θ FC	β FC
Conscious processing	Effect	Increased power at scalp and in temporal pole and pINS/HG	Decreased power at scalp and increased power in ACC and PCC	Increased fronto-temporal, cingulo-temporal and fronto-cingular FC	Increased fronto-temporal and fronto-cingular FC
	Cognitive interpretation	Information maintenance about accessed deviant stimulus	Error detection mechanisms in ACC and information integration and decision-making in PCC	Information exchange about deviant stimulus identity (fronto-temporal) and for decision-making (fronto-cingular)	Information exchange about a prediction error (fronto-temporal) for subsequent decision-making (fronto-cingular)
Subconscious processing	Effect	Increased power in pM/STG	Increased power at scalp level and in the OFC		Increased fronto-cingular FC
	Cognitive interpretation	Increased processing effort due to sensory uncertainty	Uncertainty-driven, top-down modulation signaling the need for adaption of arousal		Information exchange about a prediction error under conditions of uncertainty for subsequent arousal adaptation

Table 3. Summary of evoked oscillatory responses and functional connectivity analyses in the theta (4-8 Hz) and beta (15-30 Hz) frequency bands.

7.6. Limitations

Our findings should be interpreted keeping in mind a several caveats and methodological limitations. Our findings should be interpreted keeping in mind a few caveats and limitations. First, our analyses are limited to latencies associated with two classical auditory ERP components: the MMN and the P3. However, neural events underlying the processing of auditory deviance are by no means restricted to these arbitrarily-defined time windows. We focused on these latencies in order to related and frame evidence deriving from our study within well-grounded literature and robust findings on conscious auditory deviance detection (Bekinschtein et al., 2009; Comerchero & Polich, 1999; Garrido et al., 2009; Näätänen et al., 2007, 2011; Polich, 1987, 2007).

It could also be argued that a variable number of standard tones preceding each target could resulted in an anticipatory effect, which would be a confounding effect that could compromise our interpretation of results. It is true that such possibility cannot not be completely ruled out, but we performed control analyses which show no evidence that the number of preceding standard tones systematically modulated behavioral, electrophysiological or pupil responses across target types (annex 6).

A word of caution is also needed in the interpretation of our source-modeling results. We used a cortical template, rather than surfaces modeled after each participants anatomy, because we did not have the means to obtain individual structural anatomies for our subjects. This means that localization of neural activity reported in this work is just a broad approximation to the actual cortical regions where real neural activity might originate. Similarly, although time-frequency results in source space occur in cortical regions and oscillatory frequencies that are in line with the literature, there is still a high degree of uncertainty associated with source-modelling oscillatory activity in EEG signals.

Related to our time-frequency analyses, here we exclusively focused on the role of theta and beta oscillations in the processing of auditory deviance. However, delta and alpha oscillations have also been suggested to have an important role in gating conscious perception and sensory predictions (Arnal et al., 2015; El Karoui et al., 2015; Haque et al., 2020; Recasens et al., 2018). Investigating effects in these other frequency bands, as well as interactions across different frequencies was beyond the scope of this project. However, investigating the evoked oscillatory responses associated with the processing of sensory novelty with and without conscious access through a data-driven

approach, agnostic of arbitrarily-defined time windows or specific frequency bands, could prove useful to unveil complex cross-frequency interactions and relevant time scales for this phenomenon.

Another important issue related to functional connectivity is that many parcellations within frontal, temporal, and cingulate regions were included in our analyses which might be irrelevant for auditory deviance detection and processing. However, our results are a first approximation to a potentially more fine-grained FC analysis targeting specific cortical parcellations known to be involved in either deviance detection or processing of uncertainty. Alternatively, FC analyses could be implemented by considering functional networks rather than arbitrary anatomical parcellations. We intend to do so in the future, which was one of our motivations to initially choose a functional atlas. However, being able to relate findings to known cortical generators of ERPs as reported by fMRI literature was one of the objectives of our study, so the anatomical relabeling was a sensible analytic choice under the scope of the present thesis project.

Finally, we acknowledge that our hypothesized functional division for theta and beta oscillations FC is not fully supported by our results. There are many reasons why this is the case, ranging from potential flaws in the experimental design to a poor *a priori* definition of relevant time windows, or inherent methodological limitations. However, we offer some interesting hints that could motivate future research about this functional subdivision. We also acknowledge that our experimental paradigm is prone to improvement. Our staircase procedure, for instance, would benefit from logarithmically spaced frequencies in tonal stimuli, which could make the procedure

more faithful to human auditory perception. Similarly, it would be interesting to contrast our results with a version of our task where overt responses are not required, as to further ascertain the sensitivity of the pupil response to behavioral expectations. Notwithstanding these limitations and considering all of our reported evidence, we believe our design successfully teased apart conscious from subconscious processing of auditory deviance and could prove useful in future studies on the interaction between top-down and bottom up cognitive mechanisms with healthy and clinical populations.

8. Conclusions

We studied the brain response to auditory deviance with and without conscious access. We created a modified version of the auditory oddball paradigm that allowed us to disentangle conscious from subconscious processing of deviance. Behavioral results and replication of well-established ERP markers of auditory deviance detection with and without conscious access validate our experimental design. Moreover, source-imaging analyses show cortical activation dynamics similar to those observed in the past using fMRI, and which further confirm the identity of our ERPs of interest. Our pupillometric results demonstrate that the pupil response reflects the contribution of two components: one reflecting attentional capture and orientation to behaviorally relevant stimuli and another reflecting unexpected sensory uncertainty. However, we found no evidence that the pupil response is a reliable marker of conscious access to auditory deviance.

We observed theta power increases at the scalp level, the temporal pole and in the pINS/HG during conscious processing of deviants. This reflects information maintenance on consciously accessed deviant stimuli that would be subsequently transmitted to higher-order processors for reorientation of attention and decision-making. We also observed increased theta power in the pM/STG for subconsciously processed deviants. We propose that this reflects increased effort or cognitive load due to heightened sensory uncertainty associated with subthreshold stimuli. We also observed decreased beta power at the scalp level during conscious processing of deviance, which might reflect decreased top-down modulation when error detection is

facilitated by increased stimulus saliency. Relatedly, increased beta power in the left OFC for subconsciously processed deviants reflects top-down modulation signaling the need for arousal adaptation following unexpected sensory uncertainty. In turn, increased beta power in ACC and PCC reflects error detection mechanisms signaling the updating of internal models during conscious access to deviance.

Overall, theta power is negatively correlated with pupil size, which shows that both responses reflect sharply different cognitive mechanisms. If the ultimate goal during processing of sensory deviance is the relay of information to higher-order processors for decision-making processes and execution of overt behavioral responses, theta power reflects stimulus information maintenance about consciously accessed deviants under unambiguous sensory scenes, whereas increased pupil size reflects higher sensory uncertainty due to targets being below perceptual thresholds and the need for adaptation of brain states to meet task demands. However, it sim important to clarify that no relationship was found between beta power and pupil size, which would be expected if both responses reflected top-down modulation.

Finally we propose that functional connectivity within the range of theta oscillations during conscious processing of auditory deviance reflects information relay between regions encoding automatic auditory mismatch detection, stimulus saliency and identity and decision-making processors, which is a hallmark of access consciousness. In turn beta-band FC mostly reflects saliency-driven error-detection information exchange during conscious processing of deviance between sensory regions in the temporal lobe and cingulate and prefrontal regions encoding saliency-driven error detection. Only cingulo-temporal FC results suggest a possible role of beta

oscillations in uncertainty driven top-down modulation during subconscious processing of novelty, yet these results were not statistically significant. Time-frequency and FC results in source space do not fully support the strict functional subdivision we initially hypothesized for theta and beta band oscillations, and instead show that brain responses to novelty with and without conscious access entail more complex oscillatory dynamics.

Despite our limitations, we believe that our results illustrate the trade-off between bottom-up sensory processing and top-down mechanisms during goal-oriented and adaptive behavior and highlight the role of NE-mediated arousal adaptation in weighing neural responses to novelty and uncertainty. Our results broadly support our general hypothesis, which postulated that conscious processing of auditory deviance would be associated with increased bottom-up signals resulting from an unambiguous sensory experience, whereas subconscious processing would be characterized by increased top-down signals reflecting unexpected sensory uncertainty. However, we also found that top-down signals also encode self-generated priors in the temporal and auditory domain. Altogether, these findings illustrate the dynamic nature of the relationship between the neural mechanisms underlying perception and cognition.

9. Annexes

9.1. Annex 1

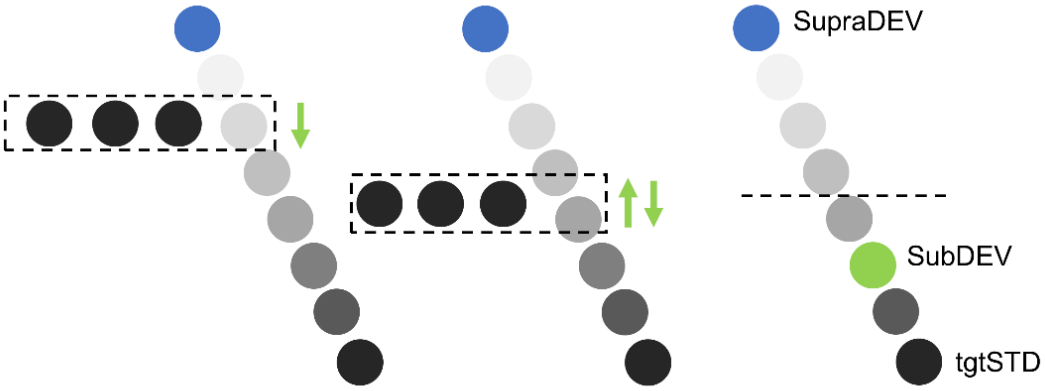

Staircase procedure. Sequences of standard tones (black circles) with a base frequency of 800, 1000, 1200 Hz were initially presented, the last of which (the target) was a tone 50 Hz above the base frequency (supraDEV target, blue circle). Participants were asked whether the last stimulus was the same or different from the rest. Every time participants responded “different”, a new trial was presented where the last stimulus would be stepped down 5Hz (left, but see table s2). Conversely, whenever, participants responded “different”, the last stimulus was stepped up 5Hz. As target stimulus was decreasingly stepped down, standard tones and target tones became increasingly similar. When participants could no longer tell the difference between standards and targets, they would enter a “same-different” loop (middle). After five iterations of this response pattern, the conscious discrimination threshold was defined as the average frequency between the two tones, and the subDEV stimulus was defined as the second stimulus below that threshold. The subDEV target was then set automatically for the immediately following block.

9.2. Annex 2

Block 1	Block 2	Block 3
850	1250	1050
845	1245	1045
840	1240	1040
835	1235	1035
830	1230	1030
825	1225	1025
820	1220	1020
815	1215	1015
810	1210	1010
807	1207	1007
805	*1205**	1005
*804**	1204	*1004**
803	1203	1003
802	1202	1002
801	1201	1001
800	1200	1000

Stimuli sets for the staircase procedure. A different set of stimuli was used for each block. Stimuli were 5Hz apart from each other down to the base frequency plus 10 Hz. Because some people can show sharp hearing abilities, the staircase jumped from 10 to 7hz, and then decreased in steps of 1Hz. In the table, asterisks represent the mode for subDEV targets across participants.

9.3. Annex 3

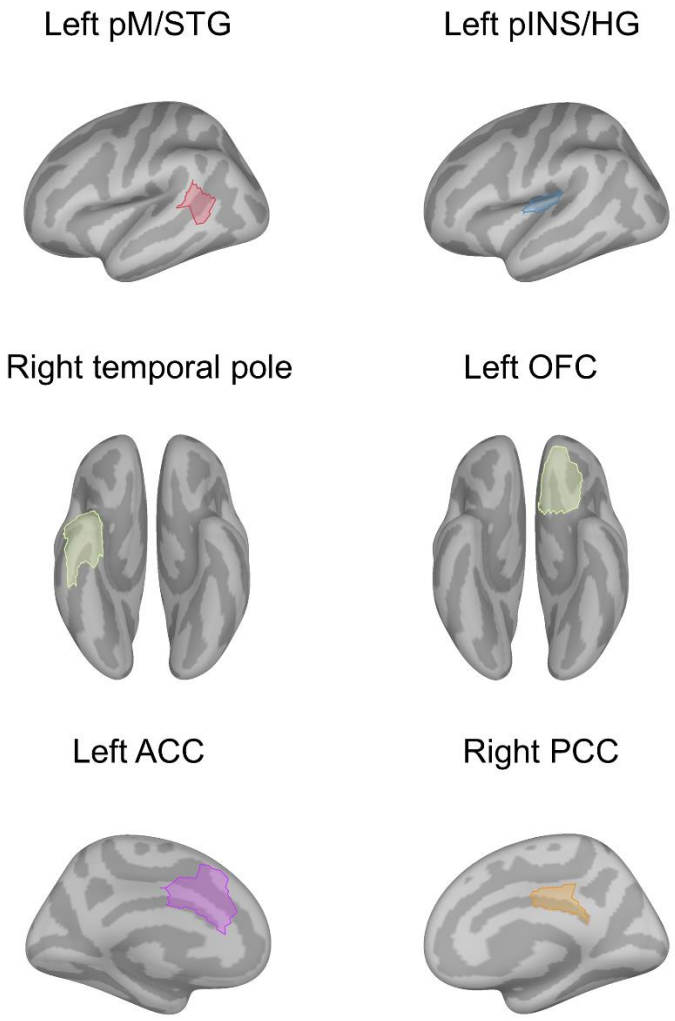

Regions of interest. Source-reconstructed regions that survive to the cluster-corrected permutation procedure. The regions correspond to parcels from the 7-network functional atlas by Schaefer et al. (2018). Labels have been corrected to reflect their anatomical location rather than the functional network they belong to.

9.4. Annex 4

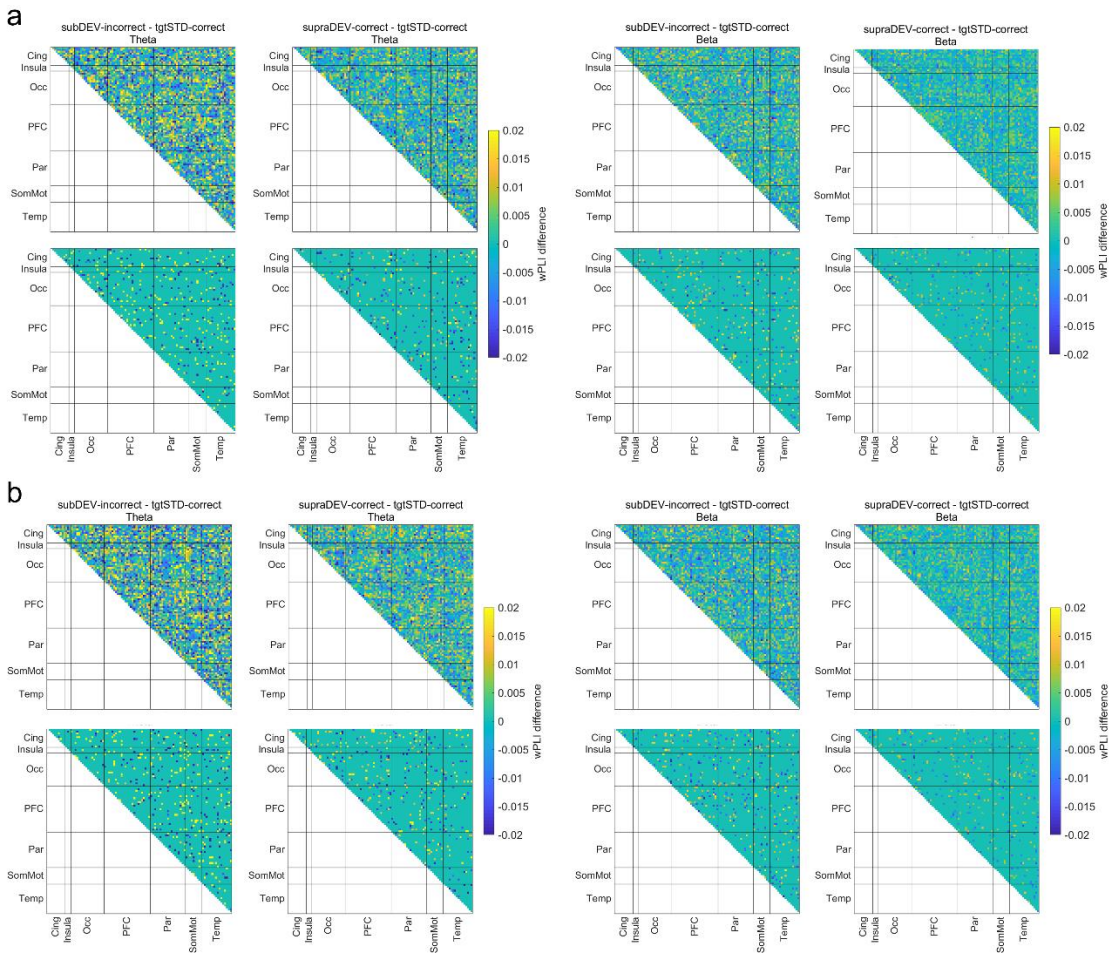

Adjacency matrices for functional connectivity (FC) values (dwPLI). a. FC for the 100 parcellations within the theta (top-left) and beta (top-right) frequency bands between 0 and 250 ms. Bottom row shows regions that survive to the 10,000 premutation procedure (above and below the 2.5 and 97.5 percentiles in the null distribution). b. as in a but shows data for the 250-500 ms time-window.

9.5. Annex 5

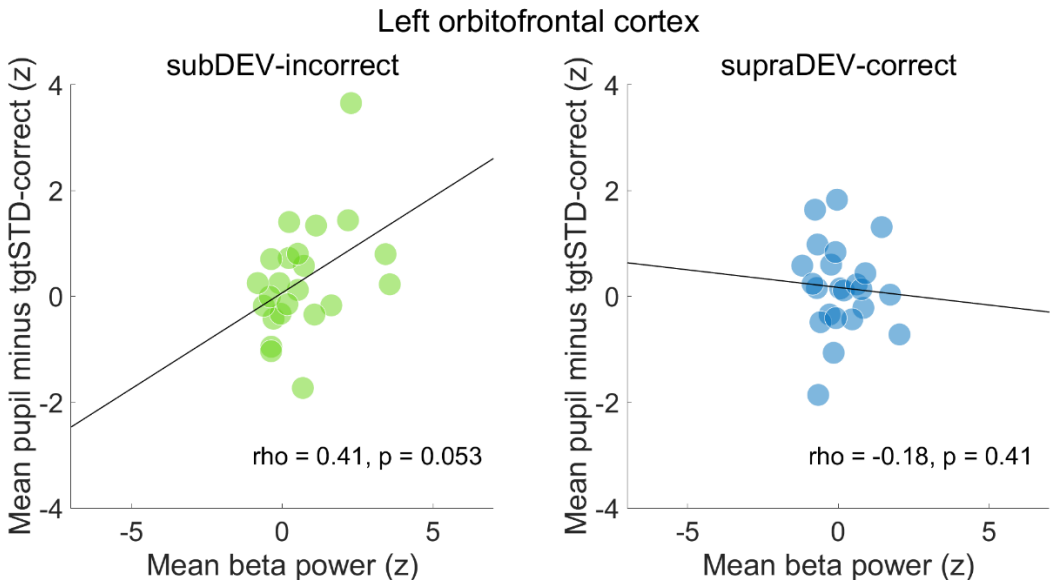

Correlation between mean pupil size difference and mean beta power between 280-380 ms in the left orbitofrontal cortex. For subDEV-incorrect trials, we found a negative association that was close to, but did not reach significance.

9.6. Annex 6

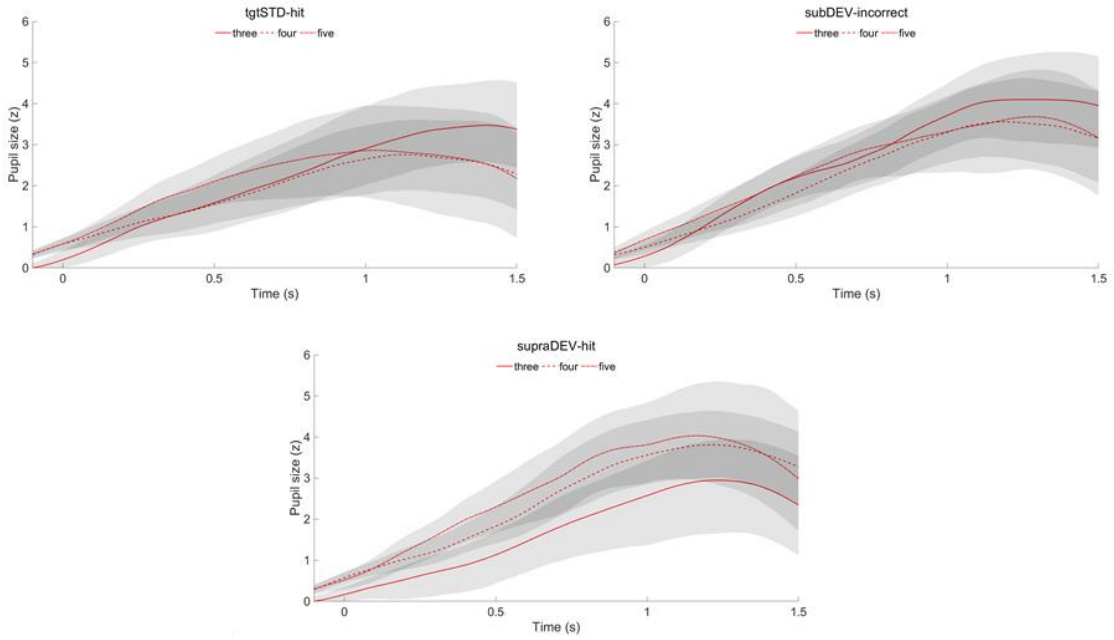

Control analysis. Pupil responses as a function of number of preceding standard tones for tgtSTD-correct, subDEV-incorrect, and supraDEV-correct trials. We found no evidence that the number of standard tones preceding each target modulated the amplitude of the evoked pupil response.

10. References

1. Akaishi, R., Umeda, K., Nagase, A., & Sakai, K. (2014). Autonomous Mechanism of Internal Choice Estimate Underlies Decision Inertia. *Neuron*, *81*(1), 195–206. https://doi.org/10.1016/j.neuron.2013.10.018
2. Alamia, A., VanRullen, R., Pasqualotto, E., Mouraux, A., & Zenon, A. (2019). Pupil-linked arousal responds to unconscious surprisal. *Journal of Neuroscience*, *39*(27), 5369–5376. https://doi.org/10.1523/JNEUROSCI.3010-18.2019
3. Arnal, L. H., Doelling, K. B., & Poeppel, D. (2015). Delta–Beta Coupled Oscillations Underlie Temporal Prediction Accuracy. *Cerebral Cortex*, *25*(9), 3077–3085. https://doi.org/10.1093/cercor/bhu103
4. Arnsten, A. F. T., & Goldman-Rakic, P. S. (1984). Selective prefrontal cortical projections to the region of the locus coeruleus and raphe nuclei in the rhesus monkey. *Brain Research*, *306*(1–2), 9–18. https://doi.org/10.1016/0006-8993(84)90351-2
5. Aston-Jones, G., & Cohen, J. D. (2005). An integrative theory of locus coeruleus-norepinephrine function: Adaptive gain and optimal performance. *Annual Review of Neuroscience*, *28*, 403–450. https://doi.org/10.1146/annurev.neuro.28.061604.135709
6. Baars, B. (1988). *A cognitive theory of consciouness*. Cambridge University Press.
7. Bachmann, T., & Hudetz, A. G. (2014). It is time to combine the two main

traditions in the research on the neural correlates of consciousness: C=LxD. *Frontiers in Psychology*, *5*(AUG), 1–13. https://doi.org/10.3389/fpsyg.2014.00940

8. Bala, A. D. S., Whitchurch, E. A., & Takahashi, T. T. (2020). Human Auditory Detection and Discrimination Measured with the Pupil Dilation Response. *JARO - Journal of the Association for Research in Otolaryngology*, *21*(1), 43–59. https://doi.org/10.1007/s10162-019-00739-x
9. Bastos, A. M., Donoghue, J. A., Brincat, S. L., Mahnke, M., Yanar, J., Correa, J., Waite, A. S., Lundqvist, M., Roy, J., Brown, E. N., & Miller, E. K. (2021). Neural effects of propofol-induced unconsciousness and its reversal using thalamic stimulation. *ELife*, *10*, 1–28. https://doi.org/10.7554/ELIFE.60824
10. Bastos, A. M., Loonis, R., Kornblith, S., Lundqvist, M., & Miller, E. K. (2018). Laminar recordings in frontal cortex suggest distinct layers for maintenance and control of working memory. *Proceedings of the National Academy of Sciences of the United States of America*, *115*(5), 1117–1122. https://doi.org/10.1073/pnas.1710323115
11. Bekinschtein, T. A., Dehaene, S., Rohaut, B., Tadel, F., Cohen, L., & Naccache, L. (2009). Neural signature of the conscious processing of auditory regularities. *Proceedings of the National Academy of Sciences of the United States of America*, *106*(5), 1672–1677. https://doi.org/10.1073/pnas.0809667106
12. Benedict, R. H. B., & Lockwood, A. (2002). Covert Auditory attention generates activation in the rostral/dorsal ACC. *Journal of Cognitive Neuroscience*, *14*(4), 637–645.

13. Berkes, P., Orbán, G., Lengyel, M., & Fiser, J. (2011). Spontaneous cortical activity reveals hallmarks of an optimal internal model of the environment. *Science*, *331*(6013), 83–87. https://doi.org/10.1126/science.1195870
14. Block, N. (2005). Two neural correlates of consciousness. *Trends in Cognitive Sciences*, *9*(2), 46–52. https://doi.org/10.1016/j.tics.2004.12.006
15. Buzsaki, G. (2006). *Rhythms of the brain*. Oxford University Press.
16. Buzsáki, G. (2010). Neural Syntax: Cell Assemblies, Synapsembles, and Readers. *Neuron*, *68*(3), 362–385. https://doi.org/10.1016/j.neuron.2010.09.023
17. Buzsáki, G., Logothetis, N., & Singer, W. (2013). Scaling brain size, keeping timing: Evolutionary preservation of brain rhythms. *Neuron*, *80*(3), 751–764. https://doi.org/10.1016/j.neuron.2013.10.002
18. Chandler, D. J., Gao, W. J., & Waterhouse, B. D. (2014). Heterogeneous organization of the locus coeruleus projections to prefrontal and motor cortices. *Proceedings of the National Academy of Sciences of the United States of America*, *111*(18), 6816–6821. https://doi.org/10.1073/pnas.1320827111
19. Chang, A., Bosnyak, D. J., & Trainor, L. J. (2016). Unpredicted pitch modulates beta oscillatory power during rhythmic entrainment to a tone sequence. *Frontiers in Psychology*, *7*(MAR), 1–13. https://doi.org/10.3389/fpsyg.2016.00327
20. Cockburn, J., Man, V., Cunningham, W., & O'doherty, J. P. (2021). *Novelty and Uncertainty Interact To Regulate the Balance Between Exploration and Exploitation in the Human Brain a Preprint*.

https://doi.org/10.1101/2021.10.13.464279

21. Comerchero, M. D., & Polich, J. (1999). P3a and P3b from typical auditory and visual stimuli. *Clinical Neurophysiology*, *110*(1), 24–30. https://doi.org/10.1016/S0168-5597(98)00033-1
22. Córcoles-Parada, M., Ubero-Martínez, M., Morris, R. G. M., Insausti, R., Mishkin, M., & Muñoz-López, M. (2019). Frontal and Insular Input to the Dorsolateral Temporal Pole in Primates: Implications for Auditory Memory. *Frontiers in Neuroscience*, *13*(November), 1–21. https://doi.org/10.3389/fnins.2019.01099
23. Dehaene, S., Changeux, J. P., Naccache, L., Sackur, J., & Sergent, C. (2006). Conscious, preconscious, and subliminal processing: a testable taxonomy. *Trends in Cognitive Sciences*, *10*(5), 204–211. https://doi.org/10.1016/j.tics.2006.03.007
24. Dehaene, S., Kerszberg, M., & Changeux, J. P. (1998). A neuronal model of a global workspace in effortful cognitive tasks. *Proceedings of the National Academy of Sciences of the United States of America*, *95*(24), 14529–14534. https://doi.org/10.1073/pnas.95.24.14529
25. Destrebecqz, A., & Cleeremans, A. (2001). Can sequence learning be implicit? New evidence with the process dissociation procedure. *Psychonomic Bulletin and Review*, *8*(2), 343–350. https://doi.org/10.3758/BF03196171
26. Ehrlichman, R. S., Maxwell, C. R., Majumdar, S., & Siegel, S. J. (2008). Deviance-elicited Changes in Event-related Potentials are Attenuated by Ketamine in Mice. *Journal of Cognitive Neuroscience*, *20*(8).

https://doi.org/https://doi.org/10.1162/jocn.2008.20097

27. El Karoui, I., King, J. R., Sitt, J., Meyniel, F., Van Gaal, S., Hasboun, D., Adam, C., Navarro, V., Baulac, M., Dehaene, S., Cohen, L., & Naccache, L. (2015). Event-related potential, time-frequency, and functional connectivity facets of local and global auditory novelty processing: An intracranial study in humans. *Cerebral Cortex*, *25*(11), 4203–4212. https://doi.org/10.1093/cercor/bhu143
28. Engel, A. K., Fries, P., & Singer, W. (2001). Dynamic predictions: Oscillations and synchrony in top–down processing. *Nature Reviews Neuroscience*, *2*(10), 704–716. https://doi.org/10.1038/35094565
29. Engel, A. K., & Singer, W. (2001). Temporal binding and the neural correlates of sensory awareness. *Trends in Cognitive Sciences*, *5*(1), 16–25. https://doi.org/10.1016/S1364-6613(00)01568-0
30. Escera, C., & Malmierca, M. S. (2014). *The auditory novelty system : An attempt to integrate human and animal research*. *51*, 111–123. https://doi.org/10.1111/psyp.12156
31. Ferguson, K. A., & Cardin, J. A. (2020). Mechanisms underlying gain modulation in the cortex. *Nature Reviews Neuroscience*, *21*(2), 80–92. https://doi.org/10.1038/s41583-019-0253-y
32. Fischer, C., Morlet, D., Bouchet, P., Luaute, J., Jourdan, C., & Salord, F. (1999). Mismatch negativity and late auditory evoked potentials in comatose patients. *Clinical Neurophysiology*, *110*(9), 1601–1610. https://doi.org/10.1016/S1388-2457(99)00131-5
33. Fonov, V. S., Evans, A. C., McKinstry, R. C., Almli, C. R., & Collins, D. L.

(2009). Unbiased nonlinear average age-appropriate brain templates from birth to adulthood. *NeuroImage*, *47*.

34. Fries, P. (2015). Rhythms for Cognition: Communication through Coherence. *Neuron*, *88*(1), 220–235. https://doi.org/10.1016/j.neuron.2015.09.034
35. Friston, K. (2012). Prediction, perception and agency. *International Journal of Psychophysiology*, *83*(2), 248–252. https://doi.org/10.1016/j.ijpsycho.2011.11.014
36. Friston, K., & Kiebel, S. (2009). Predictive coding under the free-energy principle. *Philosophical Transactions of the Royal Society B: Biological Sciences*, *364*(1521), 1211–1221. https://doi.org/10.1098/rstb.2008.0300
37. Garcia, S. E., Jones, P. R., Rubin, G. S., & Nardini, M. (2017). Auditory Localisation Biases Increase with Sensory Uncertainty. *Scientific Reports*, *7*, 1–10. https://doi.org/10.1038/srep40567
38. Garrido, M. I., Kilner, J. M., Stephan, K. E., & Friston, K. J. (2009). Clinical Neurophysiology The mismatch negativity : A review of underlying mechanisms. *Clinical Neurophysiology*, *120*(3), 453–463. https://doi.org/10.1016/j.clinph.2008.11.029
39. Gramfort, A., Luessi, M., Larson, E., Engemann, D. A., Strohmeier, D., Brodbeck, C., Goj, R., Jas, M., Brooks, T., Parkkonen, L., & Hämäläinen, M. (2013). MEG and EEG data analysis with MNE-Python. *Frontiers in Neuroscience*, *7*(7 DEC), 1–13. https://doi.org/10.3389/fnins.2013.00267
40. Gramfort, A., Papadopoulo, T., Olivi, E., & Clerc, M. (2010). OpenMEEG: opensource software for quasistatic bioelectromagnetics. *BioMedical*

Engineering Online, *9*(45). https://doi.org/10.1186/1475-925X-8-1

41. Green, D. M., & Swets, J. A. (1966). *Signal Detection Theory and Psychophysics*. John Wiley & Sons, Ltd.
42. Haque, H., Lobier, M., Palva, J. M., & Palva, S. (2020). Neuronal correlates of full and partial visual conscious perception. *Consciousness and Cognition*, *78*(December 2019), 102863. https://doi.org/10.1016/j.concog.2019.102863
43. Hautus, M. J., Macmillan, N. A., & Creelman, D. C. (2022). *Detection theory: A user's guide* (3rd ed., Vol. 4, Issue 1). Routledge.
44. Heekeren, K., Daumann, J., Neukirch, A., Stock, C., Kawohl, W., Norra, C., Waberski, T. D., & Gouzoulis-Mayfrank, E. (2008). Mismatch negativity generation in the human 5HT2A agonist and NMDA antagonist model of psychosis. *Psychopharmacology*, *199*(1), 77–88. https://doi.org/10.1007/s00213-008-1129-4
45. Horan, M., Daddaoua, N., & Gottlieb, J. (2019). Parietal neurons encode information sampling based on decision uncertainty. *Nature Neuroscience*, *22*(8), 1327–1335. https://doi.org/10.1038/s41593-019-0440-1
46. Hsiao, F. J., Wu, Z. A., Ho, L. T., & Lin, Y. Y. (2009). Theta oscillation during auditory change detection: An MEG study. *Biological Psychology*, *81*(1), 58–66. https://doi.org/10.1016/j.biopsycho.2009.01.007
47. Hyman, J. M., Holroyd, C. B., & Seamans, J. K. (2017). A Novel Neural Prediction Error Found in Anterior Cingulate Cortex Ensembles. *Neuron*, *95*(2), 447-456.e3. https://doi.org/10.1016/j.neuron.2017.06.021
48. Javitt, D. C., Lee, M., Kantrowitz, J. T., & Martinez, A. (2018). Mismatch

negativity as a biomarker of theta band oscillatory dysfunction in schizophrenia. *Schizophrenia Research*, *191*, 51–60. https://doi.org/10.1016/j.schres.2017.06.023

49. Javitt, D. C., Steinschneider, M., Schroeder, C. E., & Arezzo, J. C. (1996). Role of cortical N-methyl-D-aspartate receptors in auditory sensory memory and mismatch negativity generation: Implications for schizophrenia. *Proceedings of the National Academy of Sciences of the United States of America*, *93*(21), 11962–11967. https://doi.org/10.1073/pnas.93.21.11962
50. Jodo, E., Chiang, C., & Aston-Jones, G. (1998). Potent excitatory influence of prefrontal cortex activity on noradrenergic locus coeruleus neurons. *Neuroscience*, *83*(1), 63–79. https://doi.org/10.1016/S0306-4522(97)00372-2
51. Joshi, S., Li, Y., Kalwani, R. M., & Gold, J. I. (2016). Relationships between Pupil Diameter and Neuronal Activity in the Locus Coeruleus, Colliculi, and Cingulate Cortex. *Neuron*, *89*(1), 221–234. https://doi.org/10.1016/j.neuron.2015.11.028
52. Kamp, S. M., & Donchin, E. (2015). ERP and pupil responses to deviance in an oddball paradigm. *Psychophysiology*, *52*(4), 460–471. https://doi.org/10.1111/psyp.12378
53. Kayser, C., Petkov, C. I., Lippert, M., & Logothetis, N. K. (2005). Mechanisms for allocating auditory attention: An auditory saliency map. *Current Biology*, *15*(21), 1943–1947. https://doi.org/10.1016/j.cub.2005.09.040
54. Kersten, D., & Mamassian, P. (2004). Department of Statistics , UCLA Department of Statistics Papers Object Perception as Bayesian Inference.

Advances.

55. Kim, S., Baek, J. H., Shim, S. hoon, Kwon, Y. J., Lee, H. Y., Yoo, J. H., & Kim, J. S. (2020). Mismatch negativity indices and functional outcomes in unipolar and bipolar depression. *Scientific Reports*, *10*(1), 1–12. https://doi.org/10.1038/s41598-020-69776-4
56. Kingdom, F. A. A., & Prins, N. (2016). Signal Detection Measures∗. In N. P. Frederick A.A. Kingdom (Ed.), *Psychophysics* (pp. 149–188). Academic Press. https://doi.org/10.1016/b978-0-12-407156-8.00006-2
57. Klimesch, W., Doppelmayr, M., Yonelinas, A., Kroll, N. E. A., Lazzara, M., Röhm, D., & Gruber, W. (2001). Theta synchronization during episodic retrieval: Neural correlates of conscious awareness. *Cognitive Brain Research*, *12*(1), 33–38. https://doi.org/10.1016/S0926-6410(01)00024-6
58. Knapen, T., De Gee, J. W., Brascamp, J., Nuiten, S., Hoppenbrouwers, S., & Theeuwes, J. (2016). Cognitive and ocular factors jointly determine pupil responses under equiluminance. *PLoS ONE*, *11*(5), 1–13. https://doi.org/10.1371/journal.pone.0155574
59. Kompus, K., Volehaugen, V., Todd, J., & Westerhausen, R. (2020). Hierarchical modulation of auditory prediction error signaling is independent of attention. *Cognitive Neuroscience*, *11*(3), 132–142. https://doi.org/10.1080/17588928.2019.1648404
60. Lavín, C., Martín, R. S., & Jubal, E. R. (2014). Pupil dilation signals uncertainty and surprise in a learning gambling task. *Frontiers in Behavioral Neuroscience*, *7*(JAN), 1–8. https://doi.org/10.3389/fnbeh.2013.00218

61. Li, Y., Li-Qun Wang, & Hu, Y. (2009). Localizing P300 generators in high-density event-related potential with fMRI. *Medical Science Monitor*, *15*(3), 47–53.

62. Liao, H. I., Yoneya, M., Kidani, S., Kashino, M., & Furukawa, S. (2016). Human pupillary dilation response to deviant auditory stimuli: Effects of stimulus properties and voluntary attention. *Frontiers in Neuroscience*, *10*(FEB). https://doi.org/10.3389/fnins.2016.00043

63. Linden, D. E. J. (2005). The P300: Where in the brain is it produced and what does it tell us? *Neuroscientist*, *11*(6), 563–576. https://doi.org/10.1177/1073858405280524

64. Makeig, S., Bell, A. J., Jung, T.-P., & Sejnowski, T. J. (1996). Independent Component Analysis of Electroencephalographic Data. *Advances in Neural Information Processing Systems*, *8*, 145–151. https://papers.nips.cc/paper/1091-independent-component-analysis-of-electroencephalographic-data.pdf

65. Mashour, G. A., Roelfsema, P., Changeux, J. P., & Dehaene, S. (2020). Conscious Processing and the Global Neuronal Workspace Hypothesis. *Neuron*, *105*(5), 776–798. https://doi.org/10.1016/j.neuron.2020.01.026

66. Masson, R., & Bidet-Caulet, A. (2019). Fronto-central P3a to distracting sounds: An index of their arousing properties. *NeuroImage*, *185*(October 2018), 164–180. https://doi.org/10.1016/j.neuroimage.2018.10.041

67. Masson, R., Bidet-caulet, A., Umrs, I., Umr, C., Claude, U., Lyon, B., & Lyon, U. De. (2018). *Fronto-central P3a to distracting sounds : an index of their*

arousing properties Brain Dynamics and Cognition Team , Lyon Neuroscience Research Center (CRNL), Corresponding author . E-mail address : remy.masson@ens-lyon.fr Abstract. 1–45.

68. Miller, E. K., Lundqvist, M., & Bastos, A. M. (2018). Working Memory 2.0. *Neuron*, *100*(2), 463–475. https://doi.org/10.1016/j.neuron.2018.09.023
69. Murphy, P. R., Robertson, I. H., Balsters, J. H., & O'connell, R. G. (2011). Pupillometry and P3 index the locus coeruleus-noradrenergic arousal function in humans. *Psychophysiology*, *48*(11), 1532–1543. https://doi.org/10.1111/j.1469-8986.2011.01226.x
70. Näätänen, R., Kujala, T., & Winkler, I. (2011). Auditory processing that leads to conscious perception: A unique window to central auditory processing opened by the mismatch negativity and related responses. *Psychophysiology*, *48*(1), 4–22. https://doi.org/10.1111/j.1469-8986.2010.01114.x
71. Näätänen, R., Paavilainen, P., Rinne, T., & Alho, K. (2007). The mismatch negativity (MMN) in basic research of central auditory processing : A review. *Clinical Neurophysiology*, *118*, 2544–2590. https://doi.org/10.1016/j.clinph.2007.04.026
72. Naccache, L. (2018). *Why and how access consciousness can account for phenomenal consciousness*.
73. Nieuwenhuis, S., Aston-Jones, G., & Cohen, J. D. (2005). Decision making, the P3, and the locus coeruleus-norepinephrine system. *Psychological Bulletin*, *131*(4), 510–532. https://doi.org/10.1037/0033-2909.131.4.510
74. Oostenveld, R., Fries, P., Maris, E., & Schoffelen, J. M. (2011). FieldTrip: open

source software for advanced analysis of MEG, EEG, and invasive electrophysiological data. *Computational Intelligence and Neuroscience*, *2011*, 156869. https://doi.org/10.1155/2011/156869

75. Orr, J. M., & Weissman, D. H. (2009). Anterior cingulate cortex makes 2 contributions to minimizing distraction. *Cerebral Cortex*, *19*(3), 703–711. https://doi.org/10.1093/cercor/bhn119
76. Pasqual-Marqui, R. (2002). Standardized low-resolution brain electromagnetic tomography (sLORETA): technical details. *Methods Find Exp Clin Pharmacol*, *19*, 5–12.
77. Pearson, J. M., Heilbronner, S. R., Barack, D. L., Hayden, B. Y., & Platt, M. L. (2011). Posterior cingulate cortex: Adapting behavior to a changing world. *Trends in Cognitive Sciences*, *15*(4), 143–151. https://doi.org/10.1016/j.tics.2011.02.002
78. Perugini, A., Ditterich, J., & Basso, M. A. (2016). Patients with Parkinson's Disease Show Impaired Use of Priors in Conditions of Sensory Uncertainty. *Current Biology*, *26*(14), 1902–1910. https://doi.org/10.1016/j.cub.2016.05.039
79. Pineda, J. A., Foote, S. L., & Neville, H. J. (1989). Effects of Locus Coeruleus Lesions on Auditory , Event-Related Potentials in Monkey. *The Journal of Neuroscience*, *9*(January), 81–93. https://doi.org/10.1523/JNEUROSCI.09-01-00081.1989
80. Polich, J. (1987). Task difficulty, probability, and inter-stimulus interval as determinants of P300 from auditory stimuli. *Electroencephalography and*

Clinical Neurophysiology/ Evoked Potentials, *68*(4), 311–320. https://doi.org/10.1016/0168-5597(87)90052-9

81. Polich, J. (2007). Updating P300: An integrative theory of P3a and P3b. *Clinical Neurophysiology*, *118*(10), 2128–2148. https://doi.org/10.1016/j.clinph.2007.04.019
82. Polich, J., & Criado, J. R. (2006). Neuropsychology and neuropharmacology of P3a and P3b. *International Journal of Psychophysiology*, *60*(2), 172–185. https://doi.org/10.1016/j.ijpsycho.2005.12.012
83. Quirins, M., Marois, C., Valente, M., Seassau, M., Weiss, N., El Karoui, I., Hochmann, J. R., & Naccache, L. (2018). Conscious processing of auditory regularities induces a pupil dilation. *Scientific Reports*, *8*(1), 1–11. https://doi.org/10.1038/s41598-018-33202-7
84. Ranganath, C., & Rainer, G. (2003). Cognitive neuroscience: Neural mechanisms for detecting and remembering novel events. *Nature Reviews Neuroscience*, *4*(3), 193–202. https://doi.org/10.1038/nrn1052
85. Recasens, M., Gross, J., & Uhlhaas, P. J. (2018). Low-Frequency Oscillatory Correlates of Auditory Predictive Processing in Cortical-Subcortical Networks: A MEG-Study. *Scientific Reports*, *8*(1), 1–12. https://doi.org/10.1038/s41598-018-32385-3
86. Richter, C. G., Coppola, R., & Bressler, S. L. (2018). Top-down beta oscillatory signaling conveys behavioral context in early visual cortex. *Scientific reports*, *8*(1), 1-12. https://doi.org/10.1038/s41598-018-25267-1
87. Richter, C. G., Thompson, W. H., Bosman, C. A., & Fries, P. (2017). Top-down

beta enhances bottom-up gamma. *Journal of Neuroscience*, *37*(28), 6698-6711. https://doi.org/10.1523/JNEUROSCI.3771-16.2017

88. Rinne, T., Alho, K., Ilmoniemi, R. J., Virtanen, J., & Näätänen, R. (2000). Separate time behaviors of the temporal and frontal mismatch negativity sources. *NeuroImage*, *12*(1), 14–19. https://doi.org/10.1006/nimg.2000.0591
89. Sadaghiani, S., & Kleinschmidt, A. (2016). Brain Networks and α-Oscillations: Structural and Functional Foundations of Cognitive Control. *Trends in Cognitive Sciences*, *20*(11), 805–817. https://doi.org/10.1016/j.tics.2016.09.004
90. Sams, M., Paavilainen, P., Alho, K., & Näätänen, R. (1985). Auditory frequency discrimination and event-related potentials. *Electroencephalography and Clinical Neurophysiology/ Evoked Potentials*, *62*(6), 437–448. https://doi.org/10.1016/0168-5597(85)90054-1
91. Schaefer, A., Kong, R., Gordon, E. M., Laumann, T. O., Zuo, X.-N., Holmes, A. J., Eickhoff, S. B., & Yeo, B. T. T. (2018). Local-Global Parcellation of the Human Cerebral Cortex from Intrinsic Functional Connectivity MRI. *Cerebral Cortex*, *28*(9), 3095–3114. https://doi.org/10.1093/cercor/bhx179
92. Schapiro, A., & Turk-Browne, N. (2015). Statistical Learning. *Brain Mapping: An Encyclopedic Reference*, *3*, 501–506. https://doi.org/10.1016/B978-0-12-397025-1.00276-1
93. Slagter, H. A., Lutz, A., Greischar, L. L., Nieuwenhuis, S., & Davidson, R. J. (2009). Theta phase synchrony and conscious target perception: Impact of intensive mental training. *Journal of Cognitive Neuroscience*, *21*(8), 1536–

1549. https://doi.org/10.1162/jocn.2009.21125

94. Sohoglu, E., & Chait, M. (2016). Detecting and representing predictable structure during auditory scene analysis. *ELife*, *5*, 1–17. https://doi.org/10.7554/eLife.19113
95. Solís-Vivanco, R., Mondragón-Maya, A., Reyes-Madrigal, F., & de la Fuente-Sandoval, C. (2021). Impairment of novelty-related theta oscillations and P3a in never medicated first-episode psychosis patients. *Npj Schizophrenia*, *7*(1), 1–9. https://doi.org/10.1038/s41537-021-00146-3
96. Sutton, S., Braren, M., Zubin, J., & John, E. R. (1965). Evoked-potential correlates of stimulus uncertainty. *Science*, *150*(3700), 1187–1188. https://doi.org/10.1126/science.150.3700.1187
97. Swick, D., Pineda, J. A., & Foote, S. L. (1994). Effects of Systemic Clonidine on Auditory Event- related Potentials in Squirrel Monkeys. *Brain Research Bulletin*, *33*, 79–86. https://doi.org/https://doi.org/10.1016/0361-9230(94)90051-5
98. Tadel, F., Baillet, S., Mosher, J. C., Pantazis, D., & Leahy, R. M. (2011). Brainstorm: A user-friendly application for MEG/EEG analysis. *Computational Intelligence and Neuroscience*, *2011*. https://doi.org/10.1155/2011/879716
99. Takeshita, S., & Ogura, C. (1994). Effect of the dopamine D2 antagonist sulpiride on event-related potentials and its relation to the law of initial value. *International Journal of Psychophysiology*, *16*(1), 99–106. https://doi.org/10.1016/0167-8760(94)90046-9

100. Teixeira, M., Pires, G., Raimundo, M., Nascimento, S., Almeida, V., & Castelo-branco, M. (2014). *Robust Single Trial Identification of Conscious Percepts Triggered by Sensory Events of Variable Saliency*. *9*(1). https://doi.org/10.1371/journal.pone.0086201

101. Tiitinen, H., May, P., Reinikainen, P., & R., N. (1994). Attentive novelty detection in humans is governed by pre-attentive sensory memory. *Nature, 372*.

102. Tzagarakis, C., Ince, N. F., Leuthold, A. C., & Pellizzer, G. (2010). Beta-band activity during motor planning reflects response uncertainty. *Journal of Neuroscience*, *30*(34), 11270–11277. https://doi.org/10.1523/JNEUROSCI.6026-09.2010

103. Urai, A. E., Braun, A., & Donner, T. H. (2017). Pupil-linked arousal is driven by decision uncertainty and alters serial choice bias. *Nature Communications*, *8*. https://doi.org/10.1038/ncomms14637

104. Vazey, E. M., Moorman, D. E., & Aston-Jones, G. (2018). Phasic locus coeruleus activity regulates cortical encoding of salience information. *Proceedings of the National Academy of Sciences of the United States of America*, *115*(40), E9439–E9448. https://doi.org/10.1073/pnas.1803716115

105. Vinck, M., Oostenveld, R., Van Wingerden, M., Battaglia, F., & Pennartz, C. M. A. (2011). An improved index of phase-synchronization for electrophysiological data in the presence of volume-conduction, noise and sample-size bias. *NeuroImage*, *55*(4), 1548–1565. https://doi.org/10.1016/j.neuroimage.2011.01.055

106. Zhao, S., Chait, M., Dick, F., Dayan, P., Furukawa, S., & Liao, H. I.

(2019). Pupil-linked phasic arousal evoked by violation but not emergence of regularity within rapid sound sequences. *Nature Communications*, *10*(1), 1–16. https://doi.org/10.1038/s41467-019-12048-1

107. Zhong, L., Zhang, Y., Duan, C. A., Deng, J., Pan, J., & Xu, N. long. (2019). Causal contributions of parietal cortex to perceptual decision-making during stimulus categorization. *Nature Neuroscience*, *22*(6), 963–973. https://doi.org/10.1038/s41593-019-0383-6